tSMALL FIELD DOSE CALIBRATIONS WITH GAFCHROMIC FILM

A Thesis
Presented to
The Academic Faculty

by

Ryan J. Underwood

In Partial Fulfillment
of the Requirements for the Degree
Master of Science in the
School of Medical Physics

Georgia Institute of Technology
May 2013

SMALL FIELD DOSE CALIBRATIONS

WITH GAFCHROMIC FILM

Approved by:

Professor Dr. C-K Chris Wang, Advisor
School of Mechanical Engineering
Georgia Institute of Technology

Dr. Eric Elder
Department of Radiation Oncology
Emory University

Dr. Anees Dhabbaan
Department of Radiation Oncology
Emory University

Date Approved: April 4th, 2013.

To my mother and father: Ann and Michael Underwood.

ACKNOWLEDGEMENTS

I wish to thank my advisor, Dr. Chris Wang, for his guidance and support; Dr. Anees Dhabaan and Winship Cancer Center for the use of their equipment; Caleb Price and Anderson Cancer Institute, for letting me use their equipment; Glenda Johnson in the ME office for her administrative support when I was clueless; Dwayne Blaylock for helping me with the Georgia Tech Clinac; Chrstinia Tabor for helping me with the all the paperwork needed to use the RSEL; and Dr. Tanxia Qu (Englewood Hospital and Medical Center, Englewood, New Jersey), who first suggested the topic for this thesis

TABLE OF CONTENTS

LIST OF TABLES

LIST OF FIGURES

SUMMARY

The physics of small radiation fields in radiotherapy is discussed, as well as the need for a Code of Practice for measuring and using it. The feasibility of using Gafchromic EBT3 to accurately measure the output of these very small fields of radiation is investigated. EBT3 film is shown to be an inexpensive option for small field commissioning of therapeutic radiation devices, and is compared against other common radiation detectors.

CHAPTER I

OBJECTIVE AND MOTIVATION

Over the past decade the way that therapeutic radiation treatments for tumors are delivered has become much more precise. Technological advancements have led to treatment machines that can deliver very small and precise beams of radiation that are highly conformal. Sterotactic Radiosurgery (SRS)[1,2] and Stereotactic Body Radiation Therapy[3], as examples, are treatments that are often completed in one single fraction where a very large dose—on the order of 10-25 Gy—is delivered to one or multiple tumors in the brain or body. These special procedures utilize field sizes as small as 4mm. Other techniques such as Tomotherapy, GammaKnife, and CyberKnife[4] also deliver large amounts of radiation to very small tumors in a way that is more complicated than a traditional linear accelerator (linac).

In addition to hardware improvements, treatment planning systems (TPS) also have more complex algorithms that can generate much more complex treatment plans. Intensity Modulated Radiation Therapy (IMRT) and Intensity Modulated Arc Therapy (IMAT) use reverse-planning strategies that allow the computer to design the treatment geometry. Plans are then created that are highly conformal, and use small beamlets to deliver escalated levels of dose to the tumor, avoiding critical organs with millimeter margins for error.

The problem with these procedures though is that the physics of very small fields of radiation is not the same as that of the large fields. All of the current machine calibrations, measurement procedures, treatment algorithms and Codes of Practice are based upon theory that does not hold for very small field sizes. Most importantly, more fast electrons scatter out of the field than in, invalidating the important principle of Charged Particle Equilibrium (CPE). This leads to a reduction in dose at the target and an increased penumbra region. The reference conditions that are used for absolute dosimetry cannot then be accurately extrapolated down to very small fields. Also, small fields cannot be accurately measured with traditional ion chambers, the staple dosimetry tool used to commission treatment planning systems and perform Quality Assurance. New

dosimetry techniques and protocols therefore need to be developed that are more accurate for these smaller fields.

New QA tools have been developed for many of these special procedures. Portal dosimeters now on most linear accelerators can record a treatment plan and compare it for accuracy against the original designed plan. Other QA tools have been developed with geometry more suitable for rotational treatments like Tomotherapy and IMAT. However, these tools will only attempt to verify whatever kind of plan was designed on the computer—how can one be sure that treatment planning systems are accounting for the difference of the physics for small fields? In other words, one needs to be sure that what the computer says is going to happen will, in fact, happen.

When a treatment planning system is commissioned to work with a particular machine, whether it is a traditional linear accelerator or a GammaKnife, a large amount of measurements are taken from the machine and entered into it. One of these measurements is output factors. An output factor is a simple way of relatively comparing the output of a machine under certain settings to the output of the same machine under reference conditions where the absolute dose is known. Output factors need to be accurately measured for very small fields so that they can be used to tell the treatment planning system how the output of the machine differs when the field size gets very small, allowing it to more accurately calculate what the dose will be. But as was already mentioned, ion chambers (because of the large sizes) cannot always accurately measure the dose from very small fields. This thesis explores the pros and cons of using the GAFchromic film (International Specialty Products, Wayne, NJ) to measure the output factors of small fields.

Radiochromic film, such as GAFchromic film, has a very high spatial resolution that allows it to be used for very small fields that are difficult to measure with ion chambers. Film could potentially be an effective option if the measurement and analysis process can be optimized. By using the film, output factors from very small fields can be measured to help commission a treatment machine to be accurately used for the small fields.

Certainly, this small field commissioning process is not novel, or these special procedures wouldn't have been in use clinically. However, for smaller clinics that do not

have access to such equipment and qualified personnel, this process becomes difficult. The result is that fields below $4x4cm^2$ are avoided for IMRT/IMAT (even if they appear more optimal), and SBRT or SRS may not be utilized at all. These smaller clinics cannot use data from other clinics either, because it varies significantly based on machine and measurement strategy. There is no established protocol for general small field dosimetry to follow as of now. It is therefore the focus of this project to develop and validate a *streamlined* small field calibration procedure that can be easily and inexpensively followed.

CHAPTER II
BACKGROUND

2.1 SMALL FIELD DOSIMETRY

The term "small field" is a relative term but it is generally accepted to be any field size of 4x4cm^2 or smaller[5]. For fields this small, the physics of how the radiation is delivered is different from that of large fields and some traditional forms of dosimetry begin to fail[5]. As such, it is imperative that accurate treatment planning and QA can be performed to ensure that these very small fields are being used safely and effectively. To better understand this issue, the challenges that arise in using and measuring small fields are discussed in more detail in this chapter. These challenges serve as the evidence of the need to have a streamlined process that can be easily followed. They also explain the current long-standing state of the AAPM task groups and committees that have been tasked to tackle this problem from a macro scale. This chapter also describes the use of film in the radiation oncology clinic; including the known challenges associated with it, how it compares to other dosimetry tools, and why it is well suited to measure small fields.

2.1.1 Loss of Charged Particle Equilibrium

The biggest concern with dosimetry of small fields is the loss of charged particle equilibrium (CPE), which is a state where for every charged particle that enters a volume, another identical particle of the same energy leaves[6]. This is an important principle as the fundamental dosimetric theory states that in order to be able to calculate dose from collision kerma in the treatment volume of a given medium, CPE needs to exist. Most dosimeters, such as any type of ion chamber, are designed to be able to maintain CPE by keeping the chamber wall small enough to not significantly perturb the flow of charged particles through it. By doing so, the dose to the surrounding medium can be found using *Bragg-Grey cavity (BGC) theory*[6].

Simply stated, the ionization created in a gas filled cavity is proportional to the energy absorbed in the surrounding medium, and is found through the following relation:

$$D_{med} = \frac{Q}{m}\left(\frac{\bar{W}}{e}\right)_g * {}_m\bar{S}_g^{med} \qquad (1)$$

Where D_{med} is the dose to the surrounding medium *med* (e.g. air, water), Q is the charge accumulated in the chamber (C), m is the mass of the gas in the chamber cavity (kg), $\frac{\bar{W}}{e}$ is the mean energy spent per unit charge produced (J/C) in the cavity gas g, and ${}_m\bar{S}_g^{med}$ is the ratio of the average mass collision stopping powers of the cavity and the surrounding medium. Essentially the absorbed dose in the cavity gas is found and a proportionality factor—here the *stopping power ratio*—converts it to the absorbed dose in the medium.

In addition to the cavity needing to be small enough to maintain CPE, the other assumption of the BGC theory is that the absorbed energy in the cavity is entirely from particles crossing it[6]. It follows that for fields that are small enough, the range of the secondary electrons is large enough in relation to the chamber size that more electrons scatter laterally out of the field and deliver their dose elsewhere than are scattered in[5] (Figure 1).

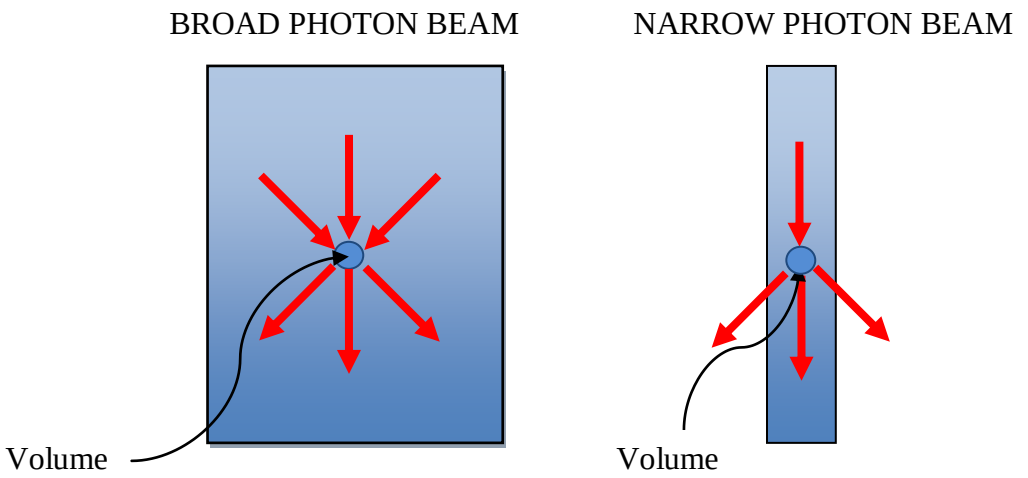

Figure 1 – A visual representation of the loss of lateral charged particle equilibrium for small fields. The fast electrons that are produced during ionization have an average range that is too large in relation to the treatment volume.

Most dosimetric measurements that are taken in the clinic use some kind of an ionization chamber and an electrometer. Instead of using Equation 1, the following relation is generally employed:

$$D_w^Q = Mk_Q N_{D,w}^{Co60} \qquad (2)$$

Where D_w^Q is the absorbed dose to water for a beam of quality Q (Gy), $N_{D,w}^{Co60}$ is the absorbed dose to water factor for the radiation quality of a Co-60 beam (Gy/C, typically), M is the charge measured on the electrometer (C), and k_Q is a constant correction factor to convert the dose factor from a beam quality of Co-60 to whatever is being used. The $N_{D,w}^{Co60}$ calibration factor is provided by a primary dosimetry laboratory when the ion chamber is calibrated—which it needs to be recently before it is used. The k_Q factor is looked up from reference tables, such as that found in TG-51[7]. The problem is that when CPE is no longer maintained, *the method by which k_Q was calculated is no longer valid*, and neither is Equation 2. k_Q is used only for making an absolute dose measurement at reference conditions, namely a 10x10cm^2 field size. There exists no reference condition for small fields that k_Q is available for.

The result of the loss of CPE is that in a small therapeutic field the resulting dose across the field will be significantly *reduced*. The measurement of the dose profile of a small field with an ion chamber suffers a phenomenon called the volume effect, which is discussed below. Two factors specifically affect the dose profile of a small field: the focal spot size, and the source occlusion, which are also discussed in the sections below.

2.1.2 Volume Effect

Because of the finite size of an ion chamber and because the dose measured is an average dose of the entire volume of the chamber, the result of an ion chamber loses its spatial resolution when the radiation field is comparable or smaller than the chamber . Typically, the result of an ion chamber is an underestimation of the dose at the center of a small field and an overestimation of the width of the penumbra at the edge of the small field. This effect is referred to as the volume effect, and is demonstrated in Figure 2.

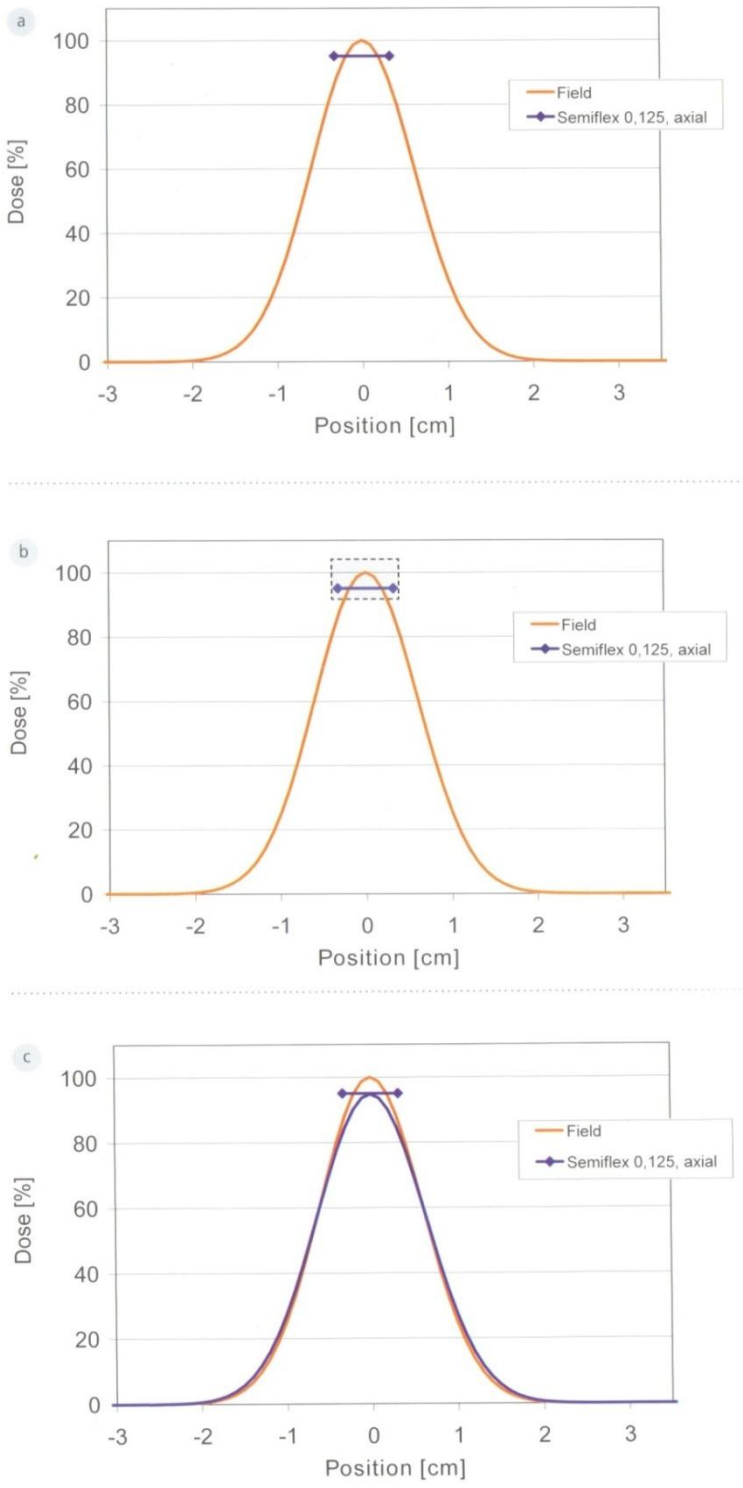

Figure 2 – A visual depiction of the volume effect with ion chambers. In this example, the ion chamber used did not have a small enough sensitive volume to accurately measure the 2x2cm field, resulting in an averaging of the dose in the center of the field and a slight overestimation of the dose in the penumbra region[8].

Because of this, if an ion chamber is to be used, it needs to be sufficiently smaller than the beam itself. Different rules of thumb exist, such as the dimension of the detector needs to be less than 25% of the field width[8]. Having reference data is critical to know whether or not absolute dose measurements in the center of the field are accurate or being reduced by this averaging. As a result of the penumbra being overestimated, the profile of the edge of a field will be smeared out, as shown in Figure 3.

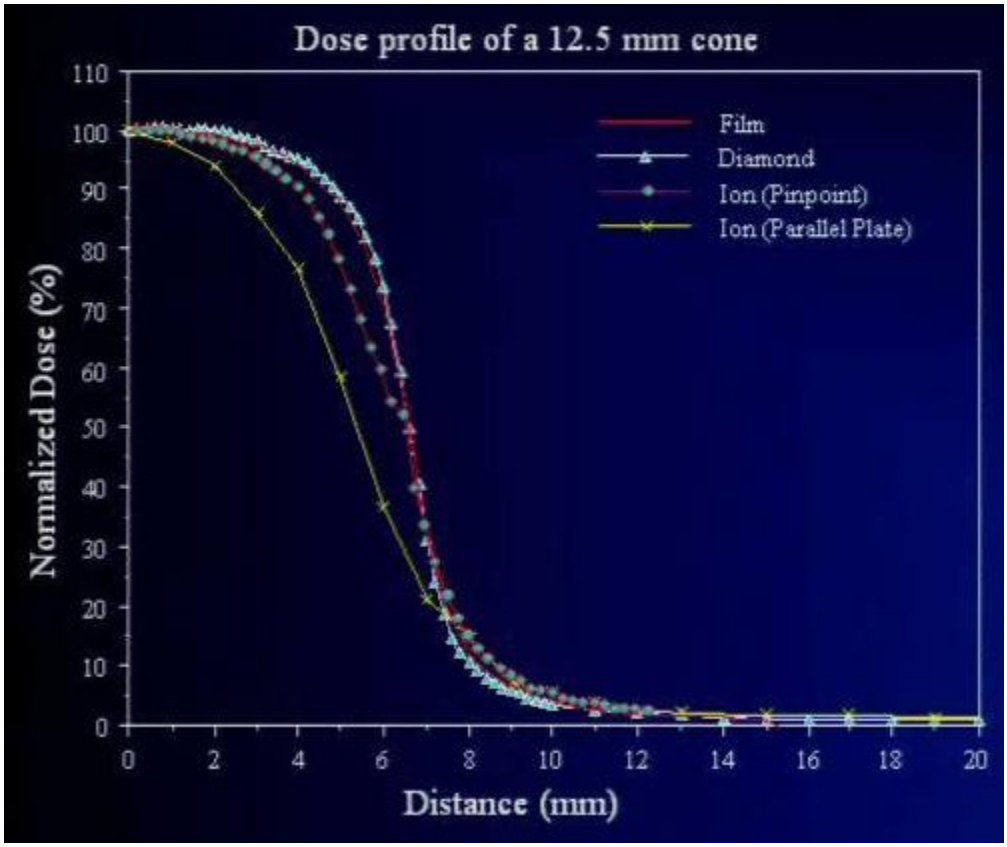

Figure 3 – It can be seen that the dose measured with the ion chambers is reduced towards the edge of the beam, and is stretched out outside of the beam due to the volume effect[9].

The impact of the volume effect can be minimized by using a very small volume ion chamber. One option is cross-calibrating a larger chamber with a smaller one[10] but the effect still exists even in the smallest available ion chamber. As such, one must consider other dosimetry tools to help minimize this problem.

2.1.3 Focal Spot Size

When the beam of accelerated electrons hits the tungsten target inside of the gantry of the linac, it produces a beam of photons with a certain finite size. The spot where the electrons hit the tungsten is called the focal spot, and it can vary in size and shape. Focal spots have been shown to vary in width between 1.5-4mm for different linacs in 6MV mode[11, 12], and their general Gaussian shape does not vary significantly over at least 2 years[13]. The shape of the focal spot can vary depending on machine and machine settings, as shown below in Figure 4.

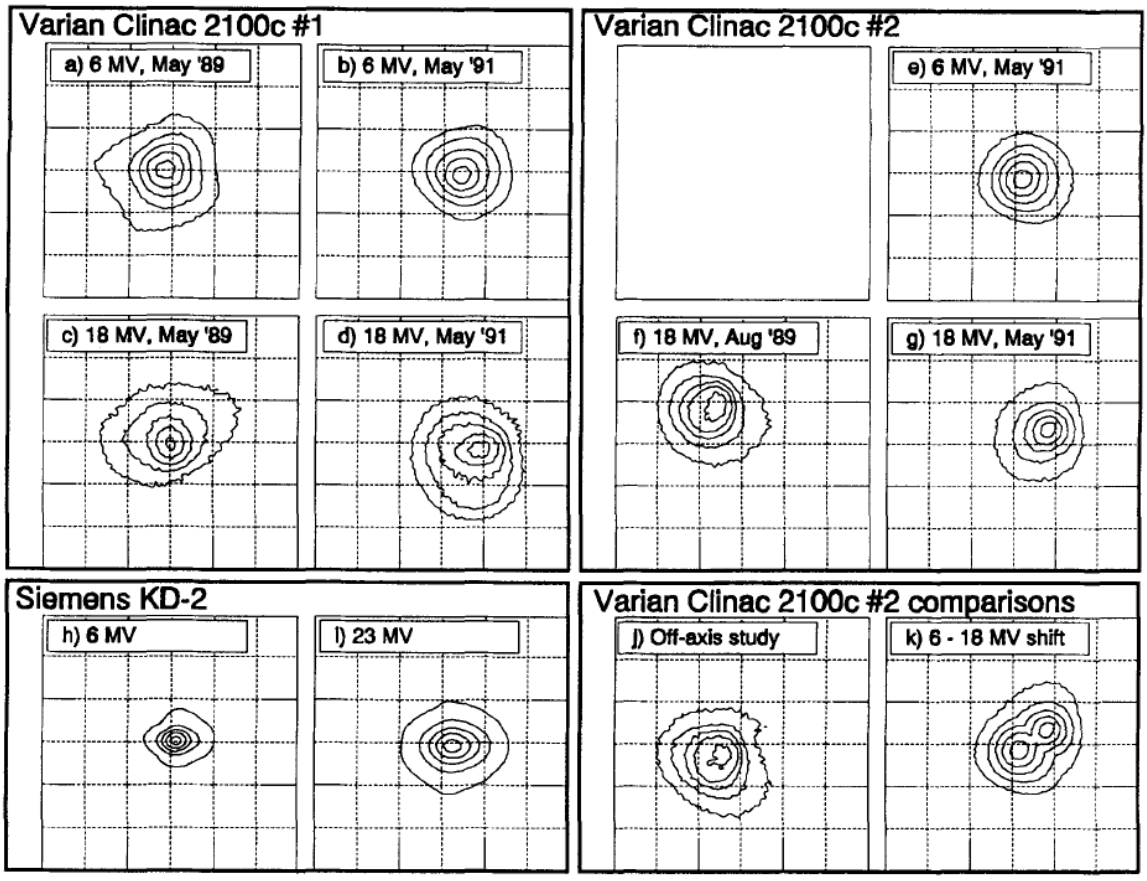

Figure 4 – Focal spot sizes for Varian Clinac 2100C (a-g, j-k) and Siemens KD-2 (h-i). The contour lines correspond to 10%, 30%, 50%, 70%, and 90% of maximum. Each small square on the grid is 1mmx1mm. Different energy modes have an effect on the focal spot, as shown in image k[13].

The shape and size of the focal spot can affect the output of a machine for very small beams. Understandably, if a field size is small enough that it approaches the size of the focal spot, precision accuracy can become very difficult to attain.

2.1.4 Source Occlusion

If the collimator jaws are set smaller than the focal spot, then the output of the machine will drop and the penumbra regions will overlap, potentially causing a significant discrepancy in the original treatment plan. This is known as source occlusion, and is visualized below in Figure 5.

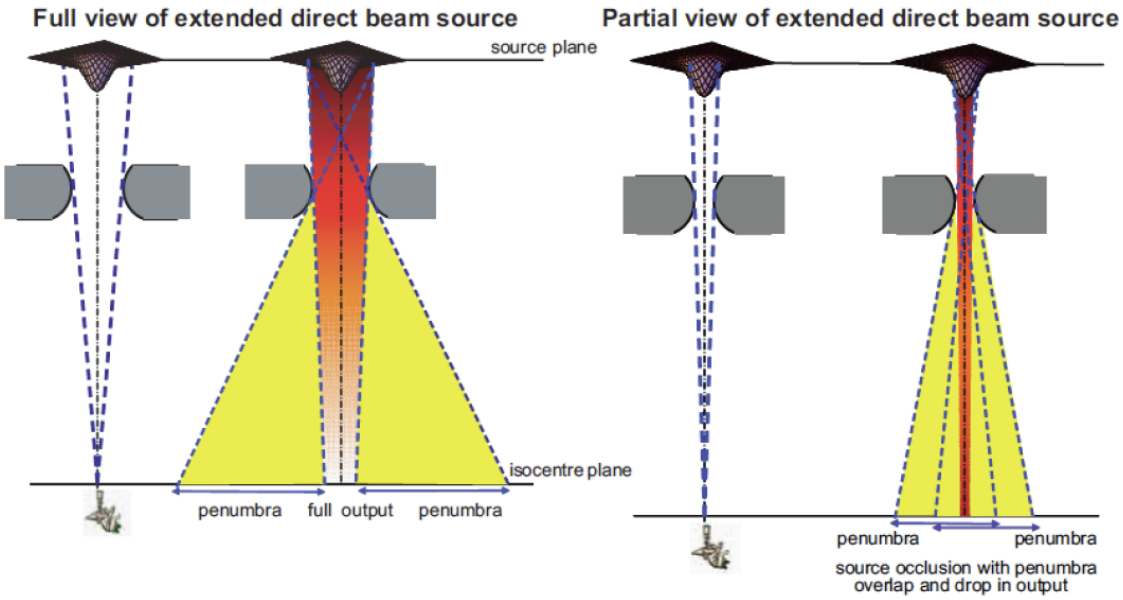

Figure 5 – Visual demonstration of the effect of source occlusion with small field sizes[14].

The term *field size* refers to the dosimetric field size, which is defined as the distance intercepted by the 50% isodose curve in the plane perpendicular to the direction of the beam, at a certain distance from the source[15]. This is not to be confused with the *geometric* field size, which is simply the field projected by the light localizer within the linac head. With the distance between the 50% isodose levels in the profile of a field being the accepted field size, the *penumbra* region is defined as the distance between the

80% and 20% isodose levels on either side of the field[15]. This results from the beam having a finite size—photon rays that originate on one side of the source may cross over to the edge of the collimator on the opposite side, essentially smearing out the dose profile of the field so it is not a perfect square (or rectangle). This can also be seen in Figure 5 as the penumbra regions begin to overlap for very small fields.

The effect of source occlusion depends on the focal spot size. Scott et al. showed through Monte Carlo calculations that increasing the focal spot size from 0.1 to 1.0mm resulted in a central axis kerma decrease of 6% for a 0.5cm field[16]. Figure 6 shows how phantom and in-air scatter factors, as well as output factors for occlusion itself, vary with focal spot size. These output factors are essentially a ratio of particular measurement conditions to reference conditions. It can be seen that source occlusion doesn't become a significant problem until fields of about 1x1cm^2 or smaller.

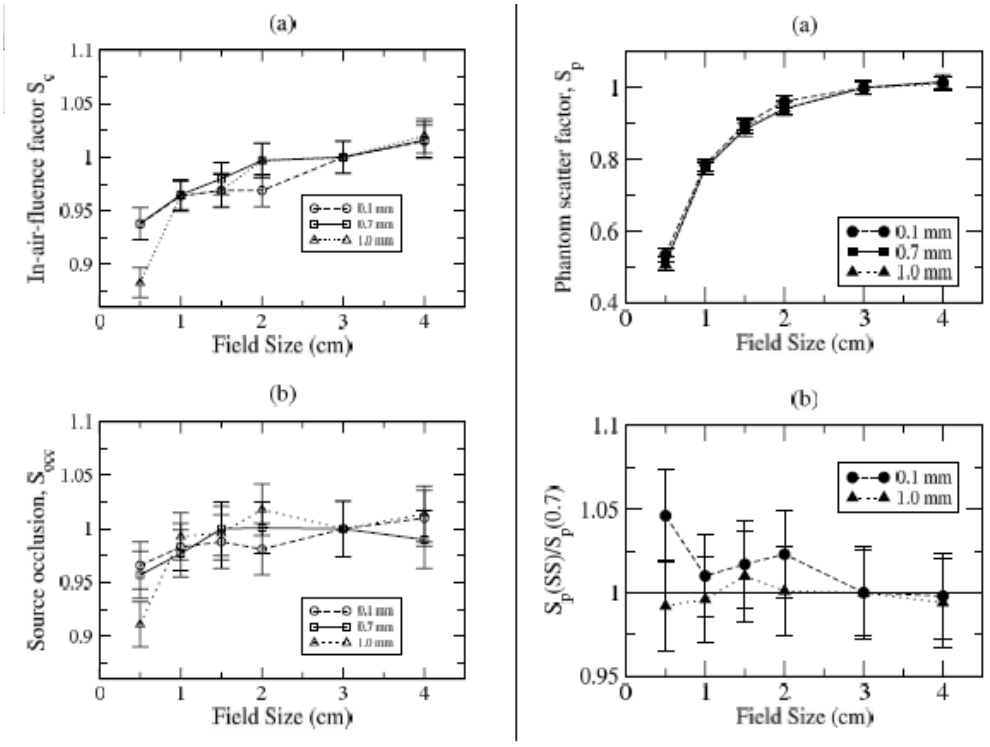

Figure 6 – The effect of focal spot size on typical output scatter factors. It can be seen that for the largest focal spot size, 1mm, the fall off of the factors is most pronounced. The image in the bottom right shows the phantom scatter factors normalized to the 0.7mm focal spot size to highlight the variation at the smallest fields[16].

2.1.5 Other Miscellaneous Concerns

When taking measurements from a linac with whichever detector is being used, the active area of the detector needs to be aligned to the center of the field. This is understandably more difficult as the field size becomes smaller. In addition to human error, it becomes very important how accurate other mechanisms are, such as: the light field projected is from the linac head, the collimator motors, the distance from the source to the detector, etc. Certain tools and software exist to assist in this, such as the PTW TRUFIX Detector Position System (PTW, Freiburg, Germany).

Some current treatment planning algorithms that correct for heterogeneities are not designed for small fields. Algorithms like Batho and equivalent pathlength primarily use the density of a medium for scaling attenuation corrections, but neglect to account for loss of electronic equilibrium or backscatter[17]. Collapsed cone convolution is capable of predicting these discrepancies, but not to the correct magnitude[18]. These inaccuracies get larger as the field sizes get smaller and smaller [17,18]. Quantitatively, the Batho algorithm has shown to produce dose deviations of 10-20% in lung tissue for a $2x2cm^2$ field[19], and the equivalent pathlength correction can have a maximum dose difference of 74% in the distal interface of an air gap[17].

There exist tertiary MLC add-ons that slide into the block tray of a linear accelerator, such as the BrainLab MMLC, which can be used for SRS. In order to reduce leakage, the sides of the leaves that touch each other have interlocking tongues and grooves, which can lead to asymmetry in the x and y dose profiles for $3x3mm^2$ fields of as much as 20-30%[20].

If a clinic cannot be confident about the accuracy of the measurements taken of small fields, then treatment plans cannot be created or used for small fields.

2.2 THE NEED FOR STREAMLINED PROCESSES

2.2.1 Output Factors

Because every linear accelerator and clinic is technically unique, accelerators need to be *commissioned* in order to be used therapeutically. Part of the process of commissioning an accelerator is measuring how the machine outputs radiation after it has been calibrated[7,21]. The output of the machine is measured under all of the different settings that the clinic would like to use, such as: field sizes, energies, photons and electrons, gantry position, and so forth. This is typically accomplished by mounting an ion chamber inside of a large tank of water, called a water phantom. Since the human body is mostly made of water, molecularly, taking the data in the water tank serves as the best guess as to how radiation would interact with human tissue. These data are used to uniquely characterize the machine so that the treatment planning software can, algorithmically, determine the dose at any point in a given volume of tissue. From this a treatment plan can then be designed and delivered with accuracy to a patient. But when taking these data, instead of going through and calculating a corrected absolute dose value for every raw electrometer reading, one uses a quantity called *output factor*.

An output factor is simply a ratio of the measured machine output in a given situation to the output under reference conditions[15]. By "output" we mean any measurement of the produced radiation per unit time: exposure rate in air, dose rate in water, energy fluence rate. One example of an output factor that is vital to know for treatment is the *collimator scatter factor* (S_c), which is defined as the "ratio of the output in air for a given field to that for a reference field (e.g. $10x10cm^2$)"[15]. The way output factors are used for commissioning is by taking the electrometer readings from all the different points inside the water phantom under a certain setup, and normalizing them to the reading at d_{max} on the central axis of a $10x10cm^2$ beam, where the absolute dose is calibrated under TG-51. This provides a relative dose measurement at all those points for the number of monitor units delivered. Computationally this makes things much simpler for taking large amounts of data. There is much more data that needs to be taken in order to commission a treatment planning system, but this thesis focuses primarily on output factors as they are the most relevant to the discrepancies that result while trying to measure small fields.

2.2.2 Variation between Detector Types

Because ion chambers are almost universally used for commissioning a treatment planning system and because ion chambers suffer from the volume effect for measuring small fields, some clinics simply avoid doing it all together. Even if a small enough ion chamber is used, the other challenges such as focal spot size and precision of positioning still pose a problem. Shown below in Figure 7 is plot of the output factors measured on a linear accelerator using different dosimeter tools[22]. The curve produced by Monte Carlo calculations serves as a control for comparison purposes.

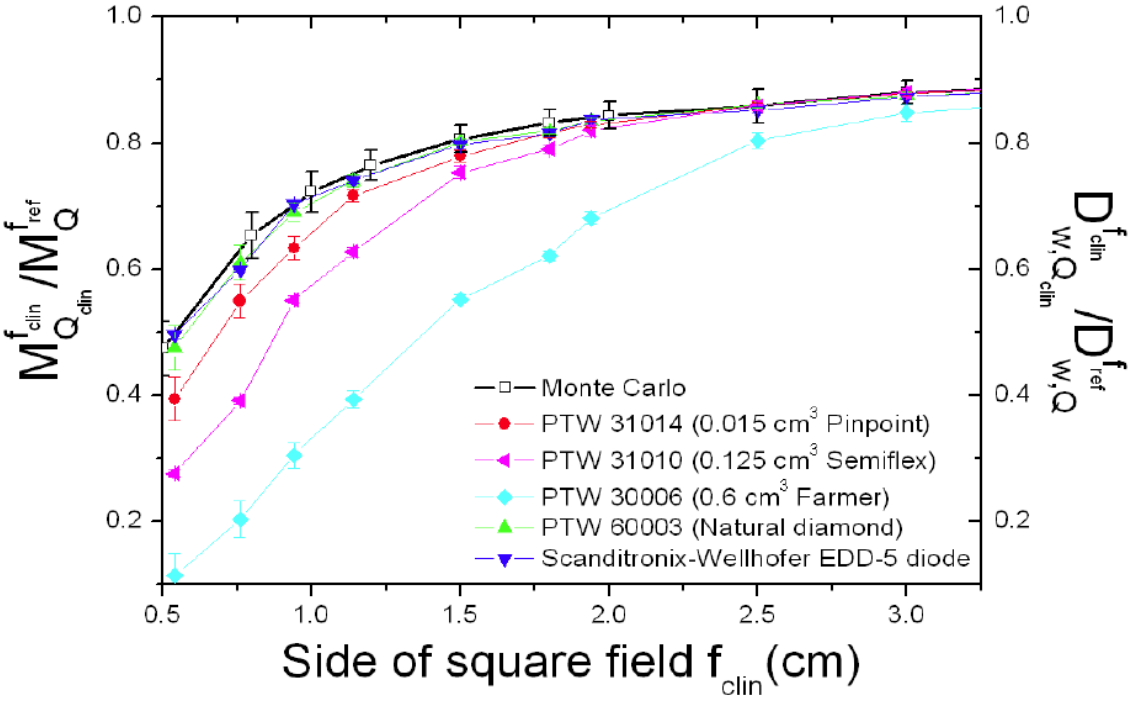

Figure 7 – Output factors found using a number of different detectors, compared to Monte Carlo calculations. The steeper fall off with the larger PTW 30006 and 31010 chambers is due to the volume effect[22].

It can be seen that the data depend significantly on what type of detector is used.

There are many different type of detectors (other than ion chambers) that currently exist, and some of them may be suitable for small field measurement. Polymer gels could potentially be used, but it would depend on the scanning technique and they haven't been shown to be the most effective option[20]. Diamond detectors are designed for

small fields and can be effective[23]. Solid state diodes have been designed for SRS dosimetric measurements, and are also more effective for small fields[23]. Radiochromic film has the highest spatial resolution of all detectors, however, and is potentially the best tool for such small fields.

2.2.3 Variation between Clinics

While measurements can vary based on what type of detector is used, they also vary between different clinics. This is because every treatment machine is slightly unique. They are subject to engineering tolerances and have many settings and characteristics that can be altered over time due to human involvement and environmental factors. Examples would include: the temperature and flow rate of the water that is used in the cooling system of a linear accelerator; the shielding design of the room, which affects scatter; gantry sag, due to gravity; the sea level of the location of the clinic can change the ambient atmospheric pressure in the treatment room; and so on. Shown below is a histogram showing the output factors measured on 45 different Novalis treatment machines, using various types of detectors. A large variation of almost a factor of 2 can be seen in the smallest fields (6x6mm).

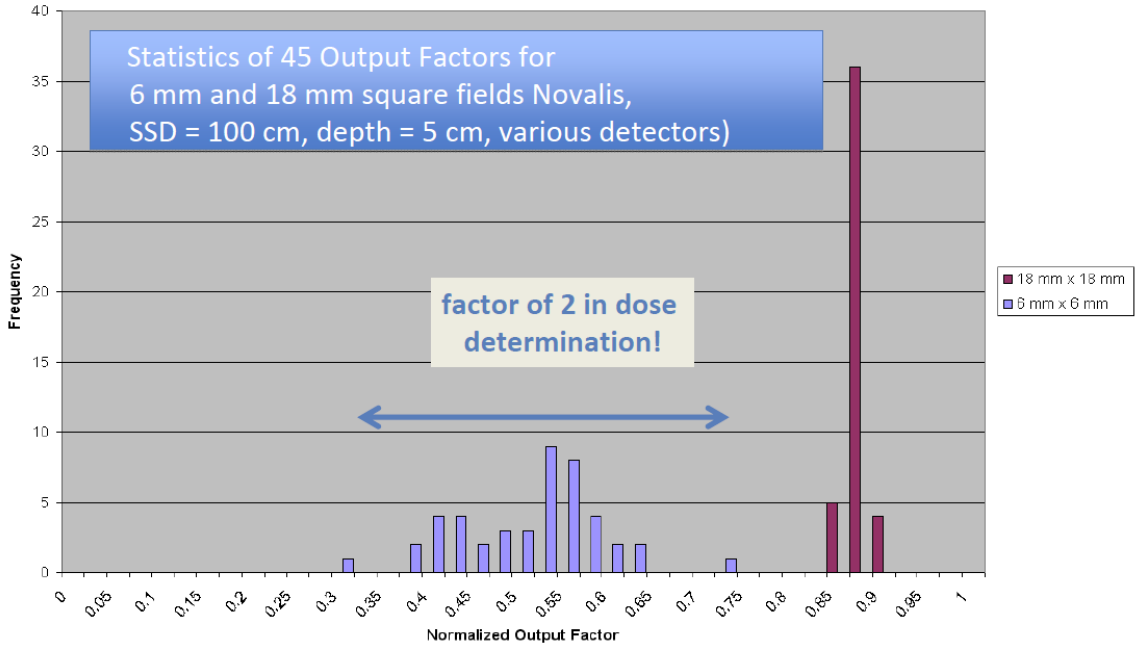

Figure 8 – Using the same measurement setup and different types of detector, output factors were found on 45 different Novalis treatment units. It can be seen that for the smallest fields, the output factors vary significantly[24].

Another figure below shows scatter factors for cones used in SRS[9]. It is clear that there is a significant variation in machine output between clinics.

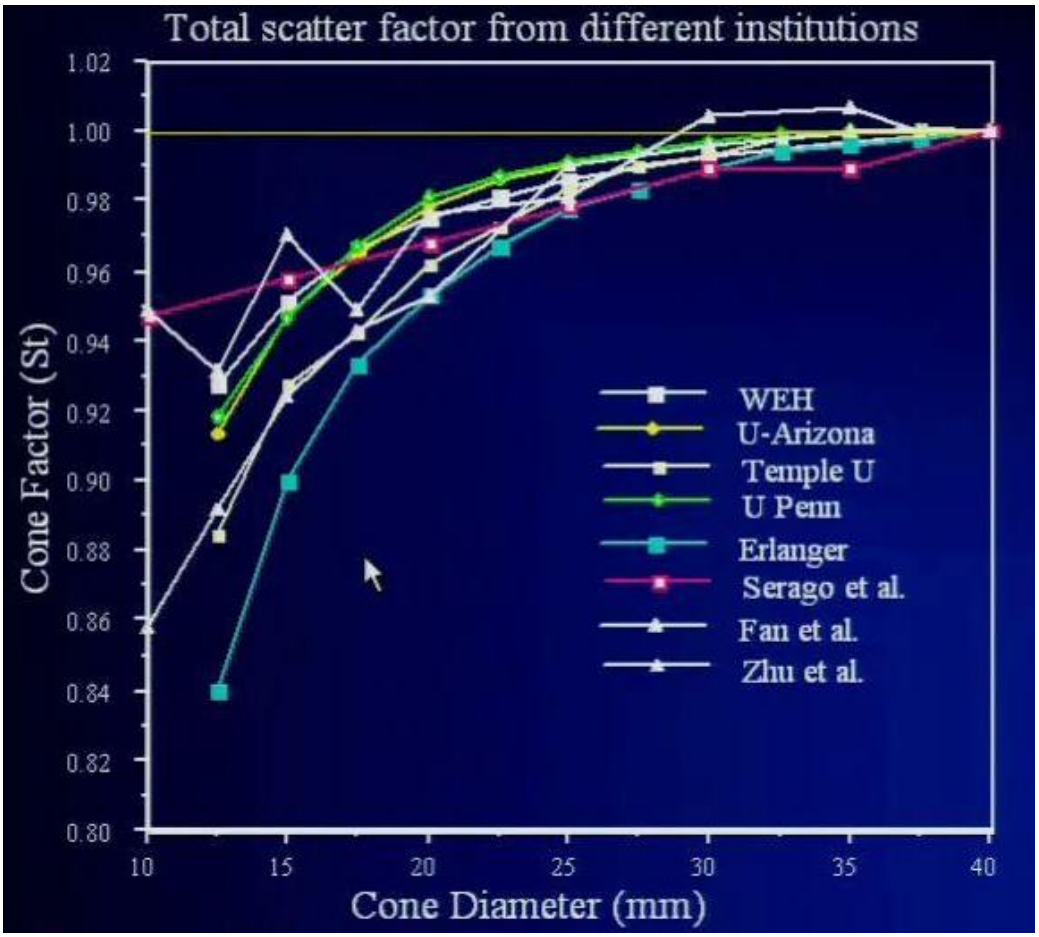

Figure 9 – Output factors to represent the influence of scatter in the use of a Radionics SRS cone for 6MV photons. Again, a large variation between clinics is noted at the smallest fields[9].

For these individual clinics that have performed their own dosimetry and commissioning, it isn't particularly important if the output of their machine is slightly different than another clinic's—all that really matters is that their unit is properly measured and characterized so that treatment plans can be delivered accurately. The problem arises, however, that not every clinic even has an onsite physicist on staff. Smaller clinics that are looking to use small fields for SRS, SBRT, electron cones, and even IMRT do not necessarily have the staff, equipment or expertise to perform this work. These figures highlight the backbone of this project all together.

2.2.4 The Need for an Established Protocol

When performing other important clinical procedures, such as an absolute dose calibration, there are established protocols that can be easily referred to such as TG-51. So instead of every clinic figuring out a solution to the problem individually, a universal procedure is followed which helps ensure that every clinic is calibrating their linac for absolute dose based on the calibration data produced for their ion chamber by a primary laboratory. However, this type of protocol does not exist for small fields on a linear accelerator; or for that matter, for: GammaKnife (Elekta Instruments, Stockholm, Sweden), Vero (Brainlab AG/Mitsubishi Heavy Industries Ltd.), CyberKnife (Accuray, Sunnyvale, CA), or Tomotherapy (Accuray, Sunnyvale, CA). It is then still up to each individual clinic to perform the dosimetry necessary to commission their equipment to be used with its respective treatment planning system. This can require transferring, extrapolating, and inter-comparing between the results of different types of detectors.

There are a number of committees that have been tasked with tackling this problem from different perspectives. The Institute of Physics and Engineering in Medicine (IPEM) released their report #103 that deals with the measurement of small field MV photon beam dosimetry[14]. The AAPM TG-178 was created in 2008 with the title: "Gamma Stereotactic Radiosurgery Dosimetry and Quality Assurance." It was charged with creating a QA and calibration protocol that could be done with typical ion chambers, and is applicable to all GSR devices. As of now this report has not yet been released, but is expected to in 2013. TG-155 was created back in 2007 to study the measurement of small field photon beams, including: protocols for commissioning TPS, the accuracy of TPS algorithms in especially inhomogeneous small fields, and correction factors for detectors. This report has also not been released yet. The AAPM Working Group on Dosimetry Calibration Protocol for Beams (WGDCPB) that are Not Compliant with TG-51 was established to collaborate with TG-155 and 178, as well as serve as a liaison to channel information to the IAEA small field committee.

2.2.5 Previous Studies

There are currently some publications on recommendations for the dosimetry of small fields—some have found correction factors for certain situations, others have proposed new calculation strategies.

Alfonso et al., including the IAEA small field committee mentioned before, proposed a new formalism for reference dosimetry for small and nonstandard fields[25]. In it they break down the relevant fields of concern into two categories: small static fields, such as the 6cm diameter collimator field with the CyberKnife, the 1.6/1.8cm diameter collimator field with the GammaKnife, and the 5cmx20cm static field with Tomotherapy; and composite fields, for any kind of dynamic or step-and-shoot delivery fields. The calculations are very similar to Equation 2, except an additional factor is included for the discrepancies with small fields. Figure 10 below depicts the formalism for small static fields:

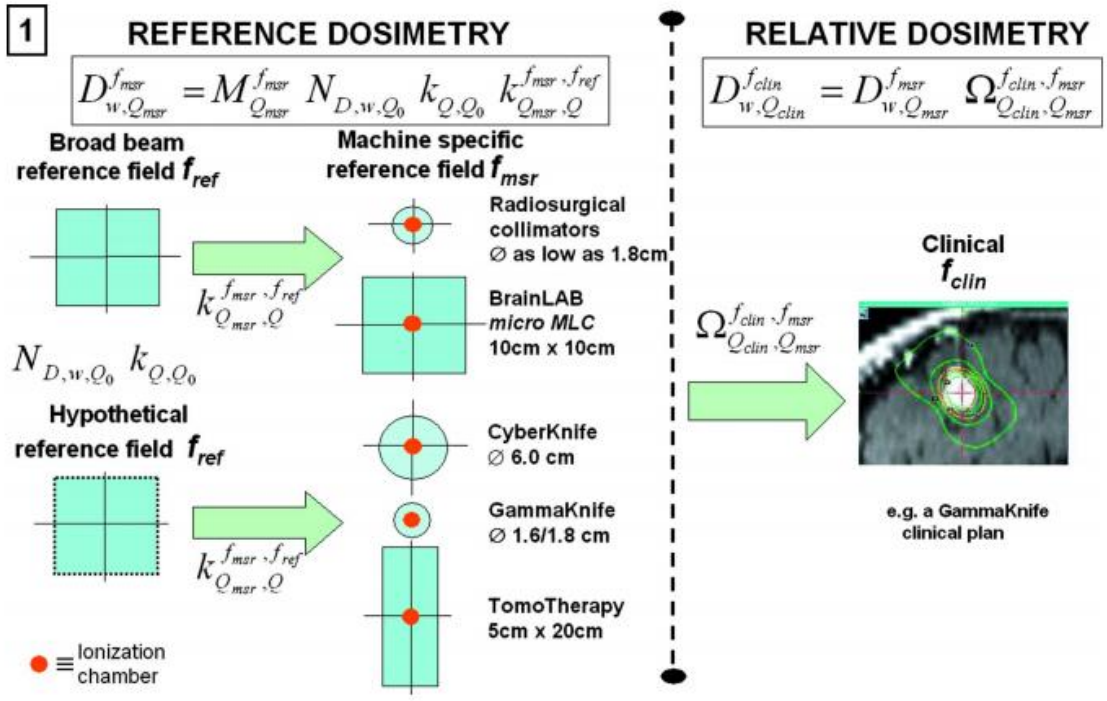

FIG. 2. Schematic overview of the dosimetry of small static fields with reference to a machine-specific reference field according to the formalism presented in this paper.

Figure 10 – The new formalism proposed for small static fields. An additional correction factor is employed to convert reference field correction factors for different small fields[25].

In this case, the subscript *msr* stands for Machine Specific Reference field, such as the examples provided (6.0cm CyberKnife, etc.). It can be seen that the ionization chamber measurements are taken and corrected the same way in the *msr* field. A correction factor for the potential difference in the beam quality for the *msr* field vs. the standard reference field is used the same way as TG-51, and an absorbed dose to water calibration factor is included the same way, for whatever reference beam quality desired—such as Co-60. However the additional correction factor is included and can be found through:

$$k_{Q_{msr},Q}^{f_{msr},f_{ref}} = \frac{D_{w,Q_{msr}}^{f_{msr}} / M_{Q_{msr}}^{f_{msr}}}{D_{w,Q}^{f_{ref}} / M_{Q}^{f_{ref}}} \qquad (3)$$

Similarly to the beam quality correction factor, this accounts for the difference in the functionality of the ionization chamber between the reference and the *msr* fields. This all makes an absolute dose calibration possible, but a correction factor is also introduced for relative dosimetry, Ω, which will not be discussed in detail here.

For composite fields, an analogous formalism is presented as follows below in Figure 11.

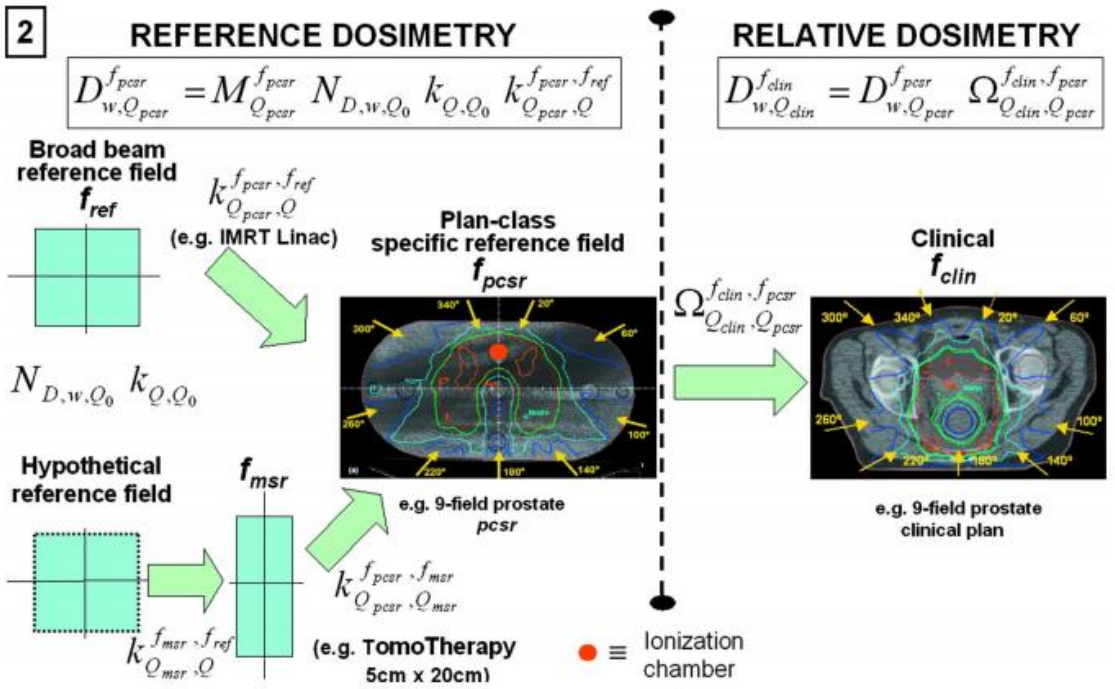

FIG. 3. Schematic overview of the dosimetry of nonstandard composite fields with reference to a plan-class specific reference field according to the formalism presented in this paper [note that in the route starting from the hypothetical field, Eq. (9) applies instead of the equation in the figure].

Figure 11 – The formalism presented for composite fields of a particular kind of treatment plan class[25].

Here the subscript *pcsr* means Plan-Class Specific Reference field, or any dynamic field or combination of composite fields that achieve CPE over time at the location of the detector. In the above figure the example of a 9-field prostate IMRT plan is shown. The correction factor from Equation 3 is first used to create an *msr* field, then the $k_{Q_{pcsr},Q}^{f_{pcsr},f_{ref}}$ factor corrects for the particular treatment setup. According to Alfonso et al, this factor will "generally be close to unity under the condition that the addition and geometrical matching of fields in the homogenous phantom compensates for the loss of charged-particle equilibrium in the penumbrae of individual fields." They calculated this factor for helically delivered treatments with different fan widths—showing it to be 1.0 or close to it in each case. Again, a relative dosimetry correction factor is introduced.

The Alfonso formalism is, however, only a guideline and has not been implemented in a clinic as an official Code of Practice. More research and data are still needed before this is the case.

There have been many studies evaluating the inaccuracies of different detectors when measuring small fields, and empirical correction factors have been calculated to help correct for them[23,25,27-29]. These sometimes rely on extrapolating from broad beams[30], mathematical models[26], or deconvolution[31]. The data and results of these reports provide solutions to specific situations, and their usefulness and applicability depend on their complexity and the resources available—in terms of both personnel and equipment/software—of any particular clinic.

Monte Carlo simulations have also been used to either calculate correction factors for particular detectors, or to directly calculate dosimetric quantities as if it were a measurement itself[32-34]. This can be particularly useful in low density or inhomogeneous mediums where experimental results are difficult to obtain[35,36]. These reports are individualistic in nature, and their biggest use may lie in the availability of relative and perhaps absolute dose control data that can be compared against independent measurements.

As of now, there is no proposed protocol or code of practice for measuring small fields using film, despite film's aforementioned advantages.

2.3 FILM AS A DOSIMETRY TOOL

2.3.1 History

Film has been used for dosimetric measurements for decades. It has also evolved over time in its chemical composition and use. The first films that were popular clinically were silver halide films from Kodak (Eastman Kodak Company, Rochester, NY). The Kodak ReadyPack XV film was popular, then CEA TVS films were shown to be more accurate and consistent[37]. Kodak Extended Dose Range (EDR) film was used and proved to be a better choice than the XV film[38]. All of these *radiographic* films required post processing in a dark room with the appropriate chemicals, and could be made inaccurate by room light. Radiochromic films helped eliminate some of these problems by the natural process of radiochromic media changing colors when exposed to radiation.

2.3.2 Gafchromic Film

Gafchromic film is a type of radiochromic film (polydiacetylene) that has become the standard in radiation oncology clinics. Gafchromic film itself has gone through many generations over the years as many different versions have been produced—a good summary of the history is provided by Devic[39]. An AAPM task group report on radiochromic film was also done and provides a more detailed history of radiochromic media[40]. The latest version of the Gafchromic film is called EBT3, and was used for this project.

EBT3 film consists of a 28μm layer containing the active component, marker dye, stabilizers and other additives. This active layer is sandwiched between two 100μm matte polyester layers. Because of the symmetric setup, the film can be irradiated and scanned without needing to keep track of which side is facing which way. The polyester has a surface treatment containing microscopic silica particles, which create a large enough gap between the scanner surface and the active layer, eliminating the interference pattern of Newton rings. The film also has 4 small holes along its edge to serve as fiducial markers, making it easier keep track of the orientation of the film during irradiation.

According to the manufacturer, the dose range of the EBT3 film is up to 10 Gy when scanning with the red color channel, the spatial resolution can resolve features to at least 25μm, the film is water resistant and can be submerged in phantoms, the yellow dye in the active layer decreases the UV/light sensitivity, and the film is near tissue-equivalent.

2.3.3 Comparison to Other Detector Types

The biggest advantage of film—regardless of what kind—will always be its spatial resolution. The resolution of ion chambers is dependent on the sensitive volume, which is on the order of several millimeters for the smallest chambers. As mentioned before, Gafchromic film can have a spatial resolution on the order of 25μm. This high resolution makes film an especially attractive option for small field work such as with SRS or measuring in high dose gradient regions with IMRT.

There are reports in the literature comparing the dosimetric abilities of film versus other common detectors[21,41,42]. With a good film dosimetry process the results are comparable to other detectors. The variation in the measurement of dose with film has decreased over time; with an optimized film dosimetry process, the variation may be as low as 2-3% now[43,44]. Because of this variation, film is not generally used in the clinic for absolute dose determination; instead ion chambers and diodes are preferred. It is used more primarily in relative dosimetry such as IMRT or HDR QA.

One problem with older generations of film was energy dependence. Muench showed back in the early nineties that silver halide films such as the Kodak XV increased in sensitivity by around 980% over the energy range of 60 kV to 4 MV x-rays[45]. EBT film has been shown to have a much smaller energy dependence—reported numbers vary, but are around 3-50% variation over a similar energy range[46-48]. The larger effect of energy dependence comes primarily from diagnostic range energies, where photoelectric effect interactions become more pronounced and are more heavily influenced by variations in high-Z materials in the active layer of the film. Within the therapeutic range this variation is only around 0.5-1%—the insignificance due to the tissue equivalence of the film[42]. Diode detectors and other non-tissue equivalent detectors are subject to a larger energy dependence[49], and care needs to be taken when choosing a detector for a given application.

Film is also inexpensive—a box of twenty five 8x10" sheets of EBT3 film costs around $400, whereas ion chambers and electrometers together can cost tens of thousands of dollars.

2.3.4 Software/Scanners That Can Be Used

Flatbed document scanners such as Epson (Seiko Epson Corporation, Owa, Japan) scanners have been used extensively with Gafchromic film[44,50,51]. The advantage of these scanners is that they are inexpensive. However they have a few disadvantages. Firstly, the measured dose will vary with the lateral location of the film on a CCD scanner[51]. This lateral response artifact is due to the asymmetric geometry and is the reason it is recommended that the film is scanned in landscape orientation, and why the film should

be placed in the center of the scanner for every film. Secondly, because these document scanners are not meant for dosimetric film measurements, it can make the process more complicated. For instance the software that comes with these scanners has different scanning modes, there are color corrections that need to be turned off, and the scanner may give you data in ADC values, which then have to be calibrated and converted into OD. There are scanners that are made solely for film dosimetry, however, such as the Vidar DosimetryPRO (Vidar Systems Corporation, Herndon, VA, USA). These scanners have been compared, and when used optimally, have been shown to be comparable[53,54].

Generally, when film is scanned into the computer the data are digitized based on what kind of mode the film was scanned. Typically scanners are operated in what is called *reflective* mode, where light is sent into the film (or document) and is reflected off the soft white material that is mounted on the lid of the scanner, where it then returns to be read by a charge-coupled device (CCD). Scanners that are made solely for film dosimetry are operated in *transmission* mode, where light is sent through the film and read directly on the other side. From this the film data are characterized as *optical density*—a scale from about 0.3-2.0—that represents the apparent opaqueness of the film.

Software that is commonly used for film dosimetry includes OmniPro (IBA Dosimetry, Schwarzenbruck, Germany), RIT (Radiological Imaging Technology, Colorado Springs, CO, USA), and a free program known as ImageJ (NIH, USA). RIT and OmniPro are designed to be able to be used directly with a Vidar scanner, which makes them an attractive option. They have many different features and options and can be used for a number of different specific tasks in the clinic, such as IMRT QA and SRS commissioning, amongst others.

There is new software called FilmQAPro, made by the same manufacturer as the EBT3 film, which uses all three color channels from the scanner for improved accuracy. Most scanners such as Vidar only use the red color channel; additionally, only the scan data from the red color channel in flatbed scanners is typically used because it is the most dose dependent and therefore most accurate. However it is claimed that the FilmQAPro uses all three color channels to separate the image into dose-dependent and dose-independent data. By averaging the response from three different color channels, it is

proposed that this will compensate for film and scanner artifacts, the lateral response of CCD scanners, and non-uniform thickness of the active layer[55,56].

2.3.5 Known Problems

There are some issues with using film in the clinic that need to be taken into account. Firstly, the orientation that the film is scanned in—landscape or portrait—can have an effect on the measured dose[46]. EBT film was shown to have a larger orientation effect than the previous Gafchromic film models, and can result in an OD difference of anywhere from 4-16%, depending on the amount of dose[46]. Since manufacturing processes are subject to certain tolerances, it is recommended that each batch of film be marked and calibrated separately. If the film from one box has run out, a new calibration needs to be performed with the new box for accuracy. One study found that the background of the films can vary by as much as 13% between batches[43].

Another discrepancy can come from the time the film is scanned after irradiation. Although the Gafchromic film does not require post processing, the opaqueness of the film does change slightly over time: up to 16% during the first twenty-four hours and around a 4% potential rise over the next two weeks[40]. Even after that the film is always becoming more opaque at a slower and slower rate. It is therefore recommended that all films be scanned at roughly the same time after irradiation.

CHAPTER III
METHODOLOGY

3.1 FILM CALIBRATION

In order for the film to be used for dosimetry it first needs to be calibrated. The correlation curve of *optical density* (OD) versus *absorbed dose* (in Gy) is accomplished through the initial calibration and is perhaps the most important step. There are a number of ways that the film could be calibrated, so the particular method discussed here is by no means the only way[57,58]. It is, however, very simple and does not require one to use very much film.

First, four 5cm blocks of solid water are placed on the treatment couch of any typical linear accelerator. They are positioned vertically so a full sheet of EBT3 film can be placed in between them, as shown in Figure 12.

Figure 12 – Calibration setup. The top of the film can be seen sticking out between the center two solid water blocks. The light field is shown as being aligned in the center of the solid water. The treatment couch is aligned so that the top of the solid water is at 100cm SSD.

The treatment couch is positioned vertically so that there is a 100cm distance between the treatment head to the surface of the solid water (SSD—Source to Surface Distance). The secondary collimator is aligned so that a 10x10cm^2 field is set. The top edge of the film should be just barely sticking out between the two solid water blocks, and the light field should be aligned such that the line where the two solid water blocks meet cuts through the middle of it. When this setup is irradiated, the resulting image on the film will represent a cross section of the beam.

Because this film was irradiated under TG-51 reference conditions, the beam data that was used to commission the linear accelerator can be used to assign dose values to corresponding depth points along the center of the film. The blocks of solid water make the setup comparable to the water phantom that was used. Clinics have this data on hand for reference, QA, and emergency calculations. Therefore, the specific energy of photons that is used is not necessarily important—as long as the beam data for that energy is available. The same could be said about field size, SSD, and even off-axis distance: as long as data is already available for a certain setting then the dose can be calculated for that point. It is for the sake of simplicity that the previously described setup is used. 6MV photons were used and 100 monitor units were delivered at a standard rate of 600MU/min. It should be noted, however, that due to the slight energy dependence of radiochromic film, a calibration film should only be used to calibrate films that were irradiated at the same energy.

The calibration film is scanned into a computer using a Vidar DosimetryPRO Advantage Red scanner. The software used on the computer to analyze the film is RIT113. Distances from the top of the film are measured in the software, and dose values are assigned, calculated from the standard MU formula:

$$Dose\ (Gy, d) = \#\ of\ MU * PDD(d)$$

where d is the depth and PDD is the percentage depth dose at d. Note that because of the setup used, no inverse square, collimator/phantom scatter, Mayneord F, or off-axis factor is required. Enough values are added so there is little space between each data point, all

the way down to the bottom of the film. The software then takes these data points and fits a curve to them, creating the desired calibration between OD and absorbed dose that can then be used for dose conversion for future films that are scanned. The calibration curve should be exponential, reflecting the inverse-square effect as the OD decreases as the depth down the film increases.

3.2 OUTPUT FACTOR MEASUREMENT

Output factors were measured using not just film, but also other common dosimeter tools for comparison. An "output factor" here is defined as a measurement of the dose at a central axis point in a given field size and depth, divided by the dose at that point for a field size of $10x10cm^2$. The film measurements were taken on the Georgia Tech Clinac iX (Varian Medical Systems, Palo Alto, CA, USA), and the Emory University Radiation Oncology Department's Novalis Tx (Brainlab AG, Freiburg, Germany). The ion chamber and diode data were taken on a Clinac EX, Trilogy, and TrueBeam (all Varian), all at the Anderson Cancer Institute's Radiation Oncology Department.

3.2.1 Film Measurements

In order to measure the actual output from the linear accelerator, some kind of phantom needs to be used. Solid water was chosen as it is easy to use and portable, as opposed to a full water tank phantom.

First the field size is set to $10x10cm^2$ in the control room. This is accomplished with the secondary collimators and not the MLC, which are disabled. One 5cm thick block of solid water is placed on top of the treatment couch. The film (EBT 3) is then centered on top of this block, and another 5cm block is placed on top of it. The top solid water block is needed for dose buildup, and the bottom block is needed for backscatter. A front pointer is used to line up the vertical position of the couch so that the top block is 100cm SSD. The top block is then removed, and the film is aligned so that the incident

light field from the gantry head is centered in the center of the piece of film. Care is then taken to place the top block directly back on without disturbing the film (Figure 13).

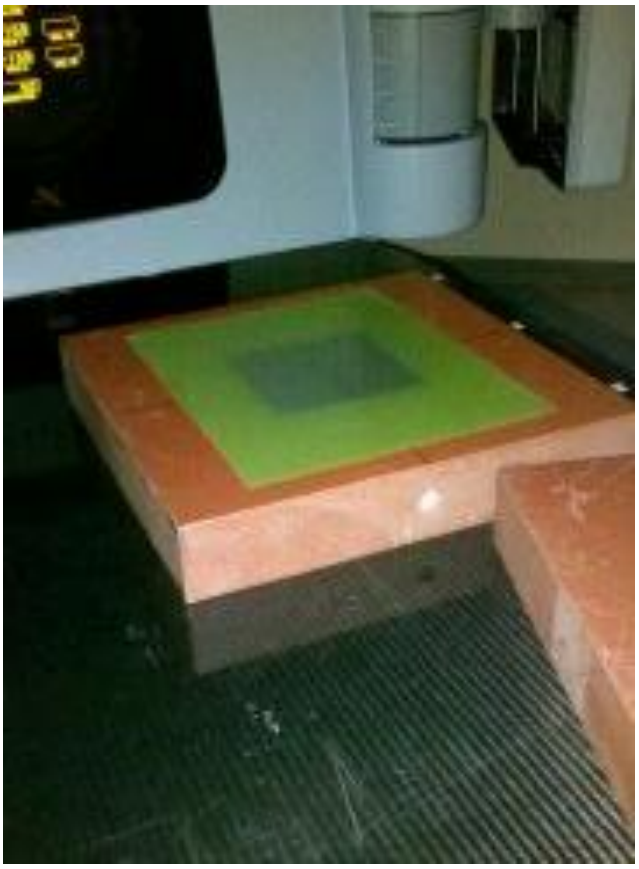

Figure 13 – Output factor measurement setup for film. The opaque square seen in the center of the film is the result of the irradiation.

Back in the control room the machine was set to deliver 200MU of 6MV photons at the same calibrating rate of 600MU/min. Once this is complete, the field size was changed to 9x9cm^2, and the previous film was replaced with a new one, again aligned properly. This process was repeated for field sizes of 8x8cm^2 down to 1x1cm^2 in 1cm increments. 0.6x0.6cm^2 field size can also be completed for newer model linear accelerators. The side of the film facing the beam was marked as "up" to distinguish itself from the other side

Once all of the films have been irradiated for the field sizes in question, they are scanned into the computer in the same way that the calibration film was. Care must be

taken to make sure to scan all of the films in the same direction and facing the same way, for consistency. Once scanned in, the calibration curve obtained before is applied, and dose values are obtained for each pixel, which in turn produces the dose profile of the entire field. A measurement cursor is placed in the observed center of the irradiation portion of the film, and a region of interest is drawn around it. The mean dose within this region of interest is measured, as shown below in the RIT screen shot.

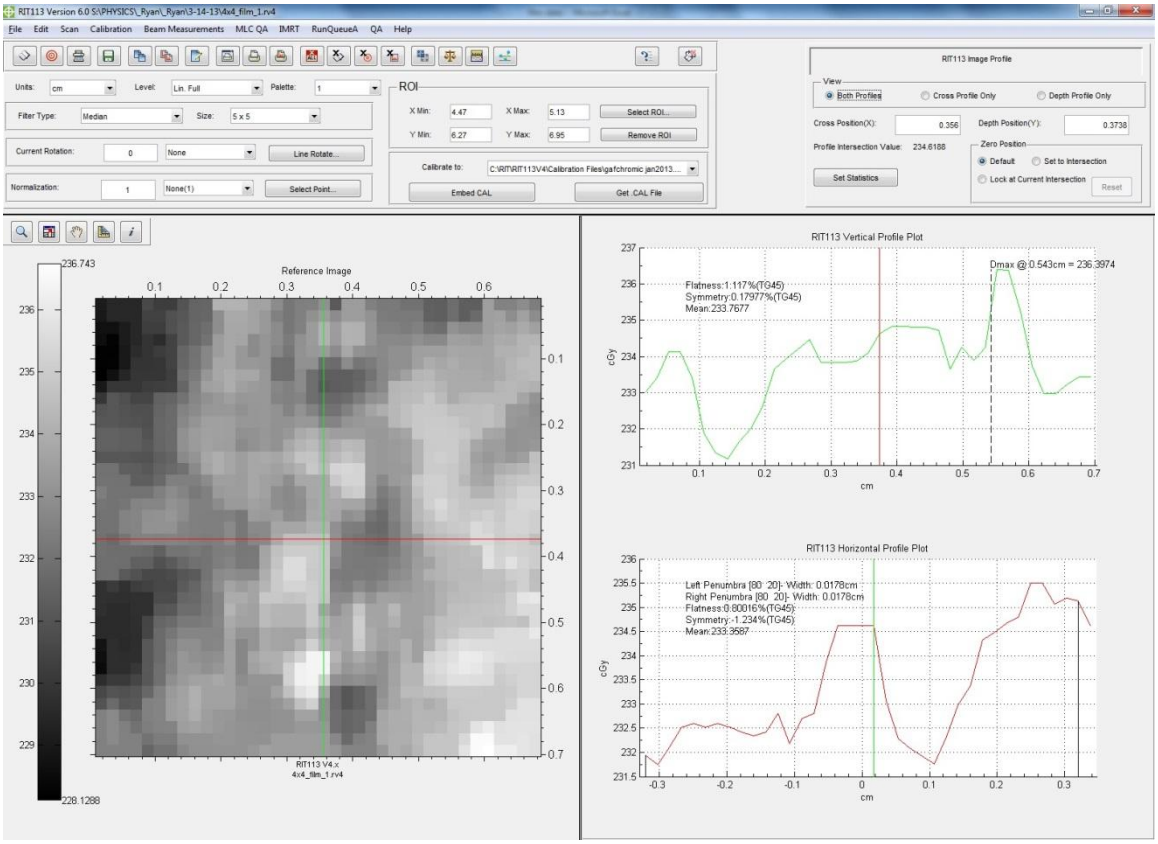

Figure 14 – Screenshot of the dose acquisition procedure on RIT. The importance of creating a region of interest is demonstrated.

It is important to take the mean dose from a region of interest in the center of the field, because as can be seen in the two cross profiles on the right side of the screenshot, the dose can vary by as much as 3%. Here the ROI drawn is about 7x7mm.

This whole process is repeated with a 1.5cm block of solid water on top, for comparison.

3.2.2 Ion Chamber Measurements

A 5cm thick slab of water has a hole drilled into it that an ion chamber can be placed into, so that the end of the ion chamber comes to about the center of the slab. The hole is in the middle of the side of the slab, making about a 2.5 depth to the sensitive volume of the chamber. There are two dark, perpendicular lines across the slab that intersect at the middle

As before, the top of the block of solid water is aligned to be at 100cm SSD, and the intersection of the dark lines is aligned to be at the center of the incident light field (Figure 15).

Figure 15 – Ion chamber measurement setup. Note that in this picture the triaxle cable from the control room is inserted into the solid water, thus why the cap is hanging out of it (an actual ion chamber was not placed inside for the picture, as it was not important). The light field is aligned to the center of the phantom.

The ion chambers used were a PTW TN30013 farmer chamber and an Exradin T1 (Standard Imaging, Middleton, WI, USA). 200MU of 6MV photons were delivered at 600MU/min. The measurement was recorded with a MAX 4000 electrometer (Standard Imaging, Middleton, WI, USA), set to a bias of -300V. This process was repeated for all field sizes used before.

Additionally, a PTW N3343 parallel plate ion chamber was taped down on top of the 5cm block of solid water from before, and the incident light field was aligned so the chamber fell in the middle of it. Because a solid water phantom designed for a parallel plate chamber was not at hand, 5cm of Super-Flex bolus (Radiation Products Design, Inc., Albertville, MN, USA) was laid over the top of the chamber, and 100cm SSD was set to the top of the bolus. The same process as before was repeated—sending 200MU for each field size, recorded with the same electrometer.

3.2.3 Diode Measurement

Finally, a Sun Nuclear Edge Detector diode (Sun Nuclear Corporation, Melbourne, FL, USA) was set up in the same way as the parallel plate chamber—taped on top of the bottom 5cm solid water block with the 5cm of super-flex bolus on top. The bias on the electrometer was set to 0V.

3.3 OUTPUT FACTOR ANALYSIS

The dose readings from the film and all the electrometer readings from each of the detectors wee inputted into an Excel spreadsheet, arranged in columns for each of the 11 different field sizes. The data for each detector was normalized to the $10x10cm^2$ field value. A plot is then created of the output factors taken with the different dosimeters in order to see how much variation there is between them. From this the comparison of the performances of different detectors can be noted by comparing to the established Monte Carlo data in the literature.

A histogram was also created, displaying all of the output factors for the smallest field sizes taken from each of the different machines with the different detectors. This

histogram help note the amount of variation attributed to the different detectors, individual machines, and setups used.

Ultimately, it is the hope that because of the superior spatial resolution of film, it will provide the most accurate output factors that could then be used for commissioning the linear accelerators used for the smallest fields.

CHAPTER IV
RESULTS AND DISCUSSION

4.1 CALIBRATION

The calibration film created is shown in Figure 16. As described in Section 3.1, the maximum dose should occur at a depth of about 1.6 cm (d_{max}), which is about 2 Gy. This is the region in the film that is the most opaque, with the highest OD. The calibration curve created on RIT is shown in Figure 17. As shown, no data points were calculated below about 60 cGy because doses this low is not of concern.

Figure 16 – The calibration film. The top of the film was the side of the film that was closest to the head of the linear accelerator, as could be deduced from the noticeable decrease in opaqueness from the top of the film in accordance with the inverse-square effect. Also the divergence of the beam can be noted as the image gets wider towards the bottom.

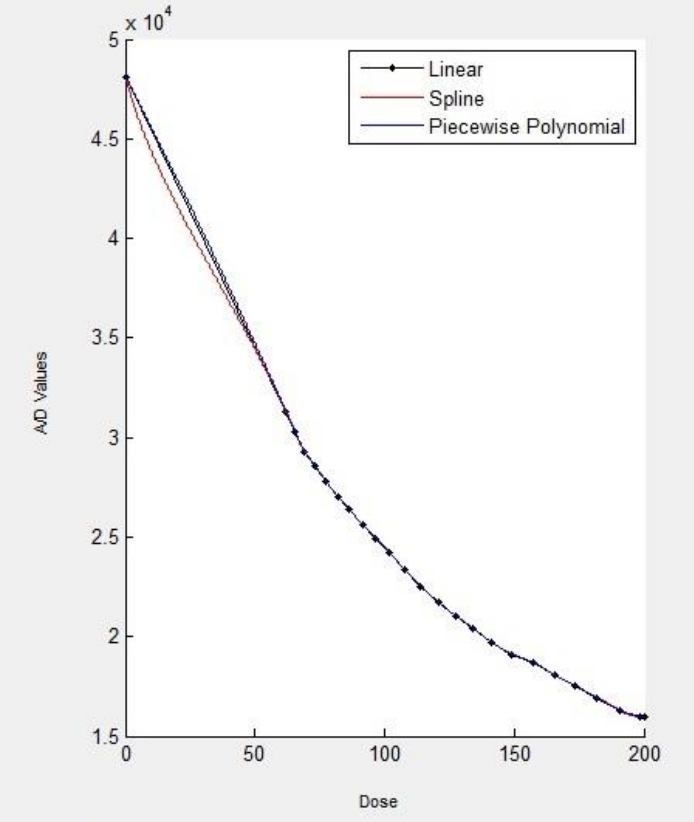

Figure 17 – The calibration curve generated in RIT. It can be seen that the data points roughly follow an exponential shape. Three different curve models are fitted to the data points: linear, piecewise polynomial, and spline. The piecewise polynomial was chosen. Note that the y-axis is A/D values, which stands for analog (to) digital, and serves as a representation of OD. The units on the x-axis are cGy.

4.2 DOSE PROFILES OBTAINED WITH FILMS

Because of the superior spatial resolution of film, the dose profiles can provide useful data. A dose profile of the 10x10 cm^2 field recorded at a depth of 1.5 cm is shown in Figure 18 as an example. It includes features such as the penumbra, flatness, and symmetry measurements performed by the software.

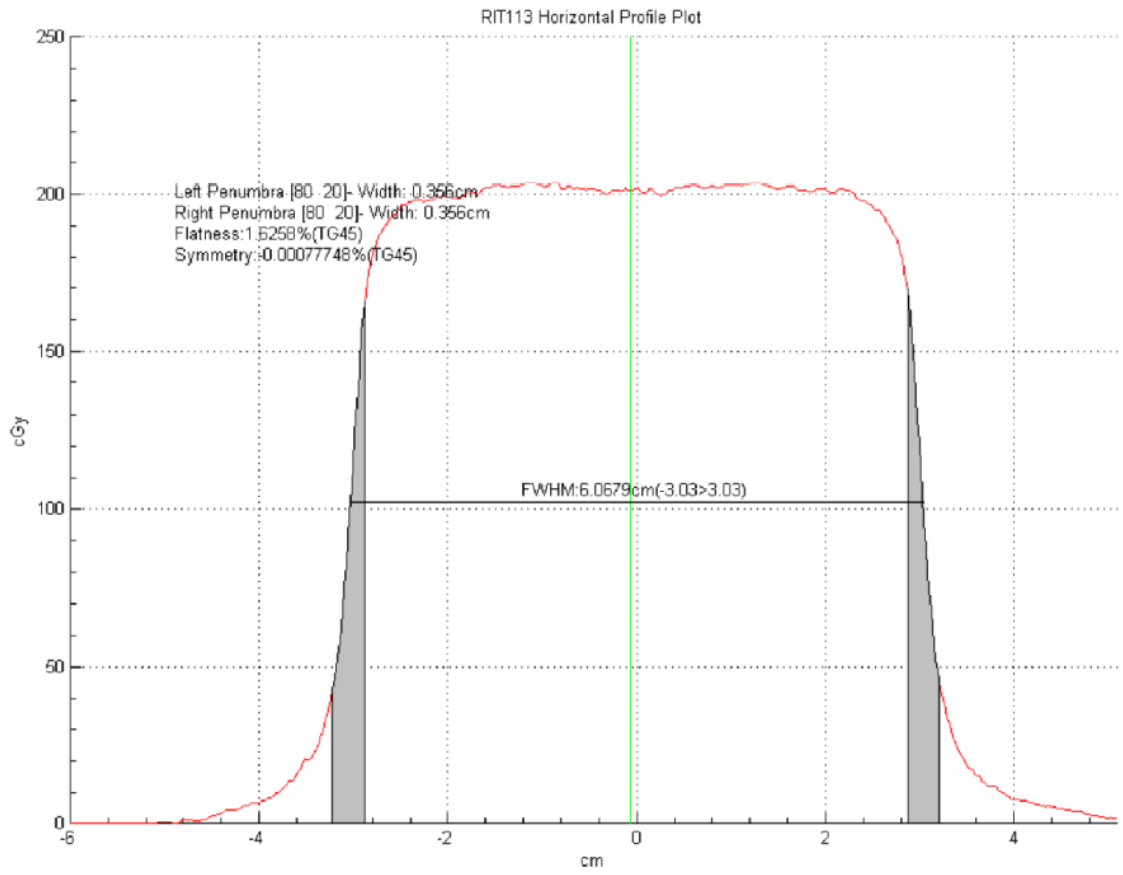

Figure 18 – The dose profile plot of the film irradiated with a 6x6cm^2 field at 1.5 cm depth, on the Georgia tech Clinac. The flatness and symmetry calculations were found by the software using the TG-45 protocol, though by convention those measurements should be found at a 10cm depth.

Because 200MU were delivered, the dose for a 10x10cm^2 field at a depth of d_{max} should be, theoretically, around 200cGy according to the TG-51 calibration. Because the OD of the film here correlated to a dose higher than 200cGy, the original calibration film created could not be used to convert OD to absorbed dose for this film. The software showed that an error had occurred and claimed that a certain percentage of the dose points are "saturated". The dose profile ended up being flat on top—truncated at 200cGy. Consequently, another calibration film was generated, except this time 400MU was delivered instead of 200. The result of Figure 18 and of other films irradiated on the Clinac iX is based on this second calibration film.

The dose measurements for the films irradiated at 5cm depth (5cm thick solid water buildup on top of film) also seemed unusual. In this instance, the maximum dose was 205cGy, which occurred in the 9x9cm^2 field. Because of the 5cm depth in "water", the dose to the film should be lower. A typical PDD value for a 9x9cm^2 field of 6MV photons at 100cm SSD, at a depth of 5cm would be around 86.6—meaning that for 200MU the dose *should* be somewhere around 200*0.866 = 173 cGy, which is 15.6% lower than the expected 205 cGy. The dose values obtained from the center of the irradiated films are summarized in Table 1.

Table 1. Absorbed dose measurements taken at center of irradiated films on Clinac iX.

Field Size (cm)	Dose at center (cGy)	
	5cm depth	1.5cm depth
0.6	129.7254	157.7911
1	143.7026	184.2329
2	168.4783	199.9754
3	167.9478	205.2239
4	184.8558	207.2164
5	176.4995	211.7215
6	189.6458	201.0911
7	181.5320	214.7890
8	199.5107	209.0799
9	205.0527	213.0583
10	199.7375	212.7800

The cause for the above mentioned discrepancy on dose results is not clear. The Clinac is properly calibrated for clinical use, and should not be the cause. As mentioned before, film has an inherent variation of around 2-5% in its dose measurements, even with an optimized dosimetry process--and quantitatively this is a feasible explanation. Since the scanner is made for film dosimetry it is unlikely there is some kind of hardware issue that could be causing this much fluctuation, although it contributes some. There could be some kind of human error in the analysis of the film with the software used. Both of these options are less likely as the film was scanned and analyzed multiple times, giving the same results.

The energy dependence of the film may be another contributor to the discrepancy. But it is relatively small, < 10% of a response difference from 60 keV to MeV range. Another contributor is associated with the scattering effect. That is, does the difference in orientation matter, between how the calibration film is irradiated and the rest of the films are? By being stacked vertically as opposed to horizontally, is the dose delivery to the calibration film different? Because the film is so thin, perhaps more of the dose to the calibration film is lower energy lateral scatter, as fast electrons are sent horizontally through it. The primary photons directed downward on it, and the electrons produced which are also more proportionally pointed downward: do they not alter to OD as much? This could help explain why the dose to the horizontally placed films is higher.

In addition to the absolute dose values being higher than expected, they also fluctuate in an odd way. As the field size gets smaller, the dose at the center of the film should be reduced slightly, and then fall off more steeply as the field sizes get very small (as can be seen in Figure 7). However here, the dose actually oscillates up and down, and the value for the $10x10cm^2$ field is not the largest.

As a final attempt to try to obtain more accurate data, the film irradiation procedure was performed again on a Novalis Tx, using a different batch of film and another new calibration film, obtained in the same way as before. The results are shown in Table 2.

Table 2. Dose measurements taken at center of irradiated films on Novalis Tx.

Field Size (cm)	Dose (cGy, Portrait)
0.6	158.6
1	192.3
2	214.0
3	219.2
4	223.7
5	230.7
6	236.8
7	237.3
8	240.4
9	240.3
10	244.5

As shown, although the data still seem higher than they should be, they no longer oscillate like before. The dose slowly decreases then falls off the fields below 4x4cm^2, as expected.

Ultimately, because output factors are a relative comparison, the absorbed dose is not important for them. If all of the doses are higher or lower than expected, but are so proportionally, then the output factors will not change. And in terms of commissioning, as long as the dose is known, whatever it may be, then the machine could still be used accurately.

The variation in dose measurement of film can be noted along the top of the profile of Figure 18. Many QA protocols for clinics follow the AAPM TG-142 recommendations for flatness and symmetry maximum allowable changes of about 1-2%[59]. For this particular field the quality of the beam would fail. However, the film very accurately displays the dose fall off in the penumbra region—a big reason why it is used for QA in the clinic. As mentioned in Section 2.1.4, the field size is defined as the distance between the 50% isodose levels. Here the FWHM of the profile is close to that.

In order to highlight the effect of small fields, the dose profile of the 6x6mm^2 field at 5cm depth is shown in Figure 19.

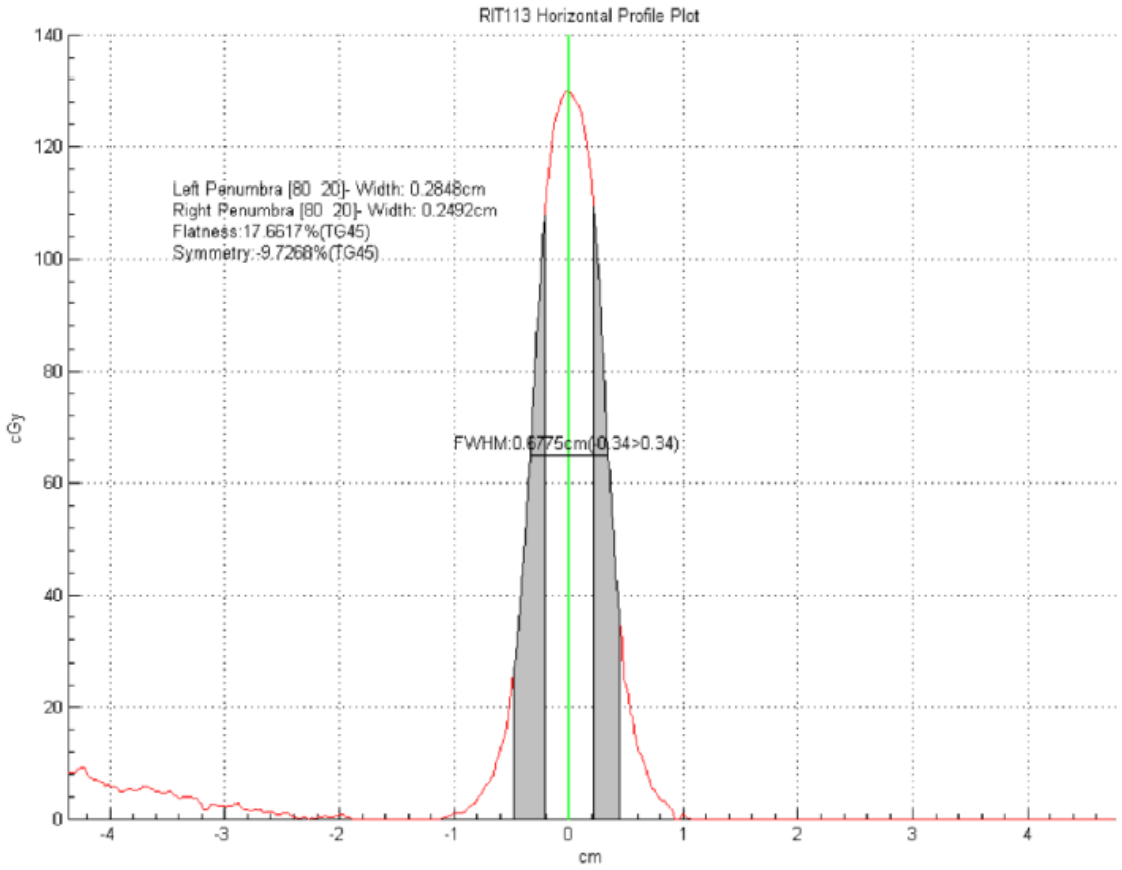

Figure 19 – The dose profile of the 6x6mm^2 field film at 5cm depth. The aforementioned effects of small field physics are evident, as the dose to the center of the field is reduced.

It is observed that the absorbed dose value on the central axis is significantly reduced, and the profile is no longer flat. However the FWHM of the profile is still close to the field size, and the penumbra regions (defined in Section 2.1.4) are actually slightly reduced due to the smaller size of the field itself. The slight increase in dose on the left side of the film is unclear.

Figure 20 shows a plot of the flatness, symmetry, right and left penumbra for each of the films irradiated at the 1.5cm depth.

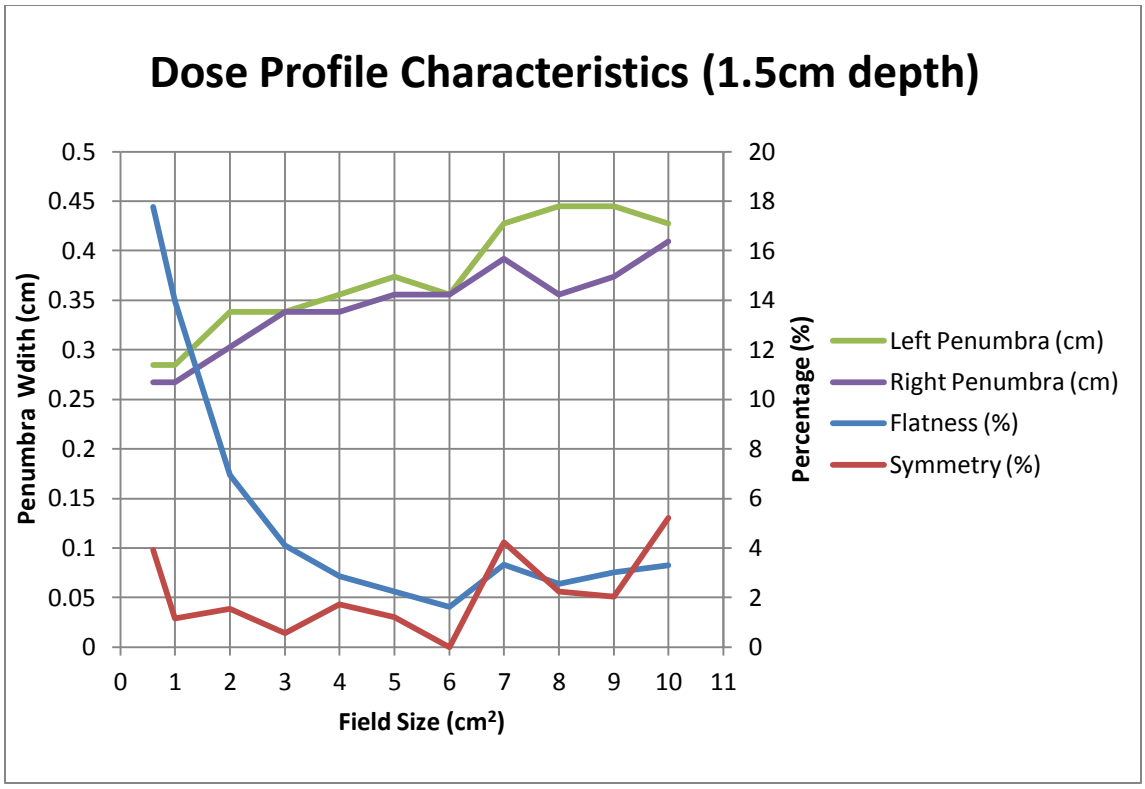

Figure 20 – Penumbrae, flatness, and symmetry calculations from the films irradiated at 1.5 cm depth. The flatness decreases with field size as lateral scatter become more pronounced, and the right and left penumbra are similar across the field sizes.

As shown, the right and left penumbra are similar and do not deviate significantly—a result of the symmetry of therapeutic beams. There appears to be no real correlation between symmetry and field size. These symmetry percentages are likely higher than what would actually be present in the beam, due to the variation of film. The flatness of the beam decreases significantly with field size, due to lateral scatter rounding out the dose profile. Note that the flatness percentage doesn't increase significantly until below 4x4cm^2 field size, which supports the common definition of a "small field".

Finally, the dose profile characteristics of the films irradiated at 5cm depth are shown in Figure 21. The results are comparable to that of the films irradiated at 1.5cm depth, except the symmetry percentage of the 6x6mm^2 field is very poor, due to the slight increase on the left side of the dose profile shown already in Figure 19. Also because of some noise on the left side of the 10x10cm^2 film, the penumbra value is skewed and was

not included here. In general, the symmetry measurements were higher for the larger field sizes.

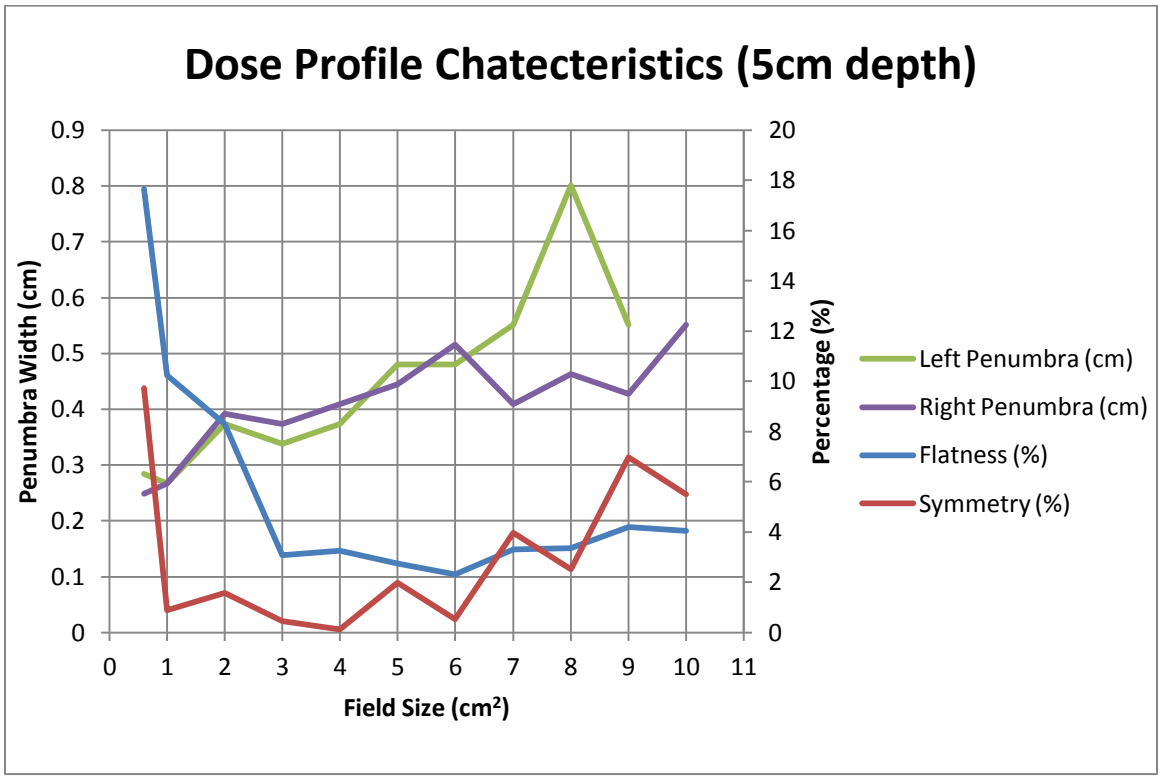

Figure 21 – Dose profile characteristics of the film irradiated at 5cm depth on the Georgia Tech Clinac. The left penumbra of the 10x10cm field is not shown because of some error on the side of the film.

4.3 VARIATION BETWEEN DETECTOR TYPES

The output factors measured with the Gafchromic film are shown in Figure 22. Compared to the data in the literature, such as in Figure 7, the film result is quite good. As shown, the dose drop from the large field sizes to small field sizes is not very linear. The Monte Carlo results shown in Figure 7 show that the output factors should drop off exponentially for field sizes below 4x4cm^2 to around 0.5 for a field size of 6x6mm^2. The spatial resolution of the film proved to be advantageous at these small fields, as hoped.

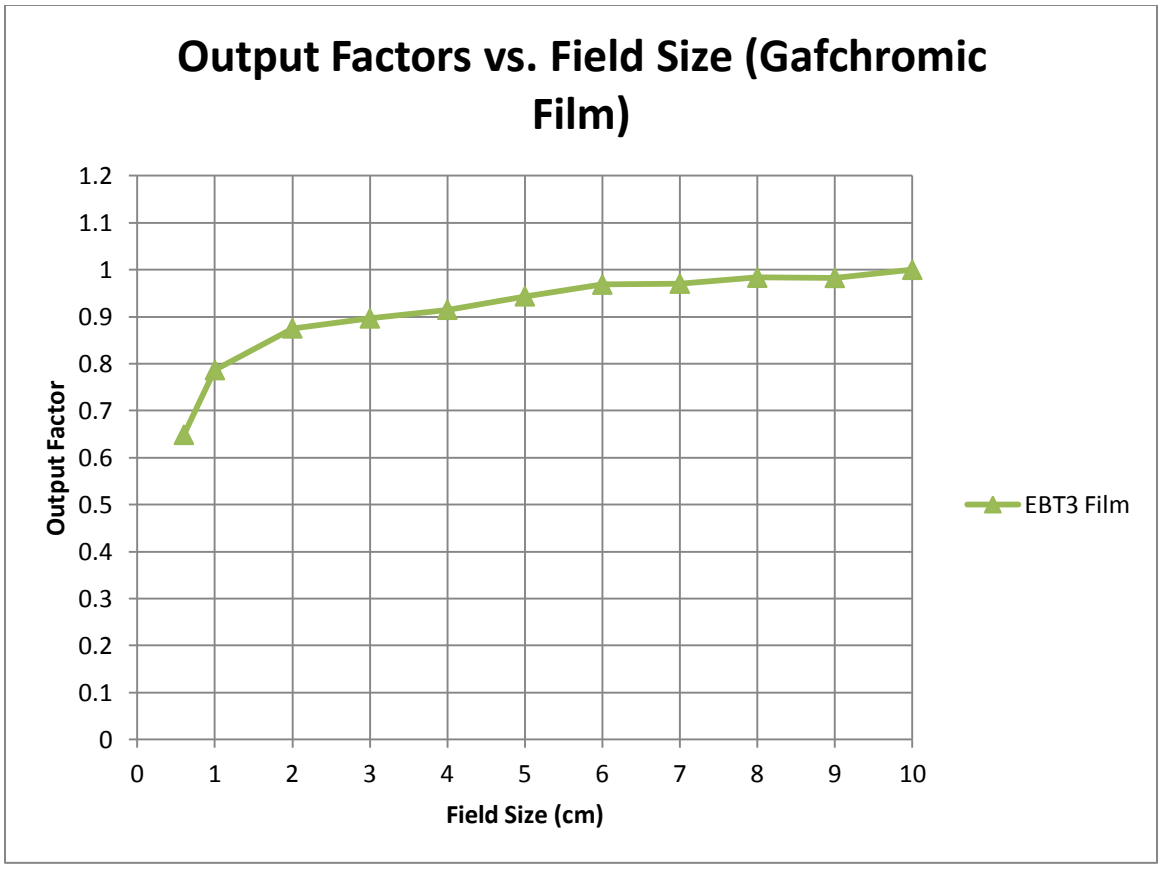

Figure 22 – Output factor data measured on a Novalis Tx with the EBT3 film. It can be seen that the results closely mimic the data obtained from other reports, such as in Figures 7 and 9, for how the output is affected by very small field sizes.

The film output factors shown in Figure 22 are the data obtained from the 4th measurement trial, taken on the Novalis Tx. The output factors calculated from the film irradiated on the Clinac did not turn out accurately, and are not shown here. A summary of what caused this inaccuracy is described in detail in Appendix A.

As discussed before, some detectors are more suitable to measure small fields than others. Figure 23 shows the output factors measured on a Varian TrueBeam linac. The detectors used were the Exradin T1 ion chamber, Edge Detector, a parallel plate chamber, and a farmer chamber. All measurements were taken by the processes described in Section 3.2. The film data are included for comparison purposes.

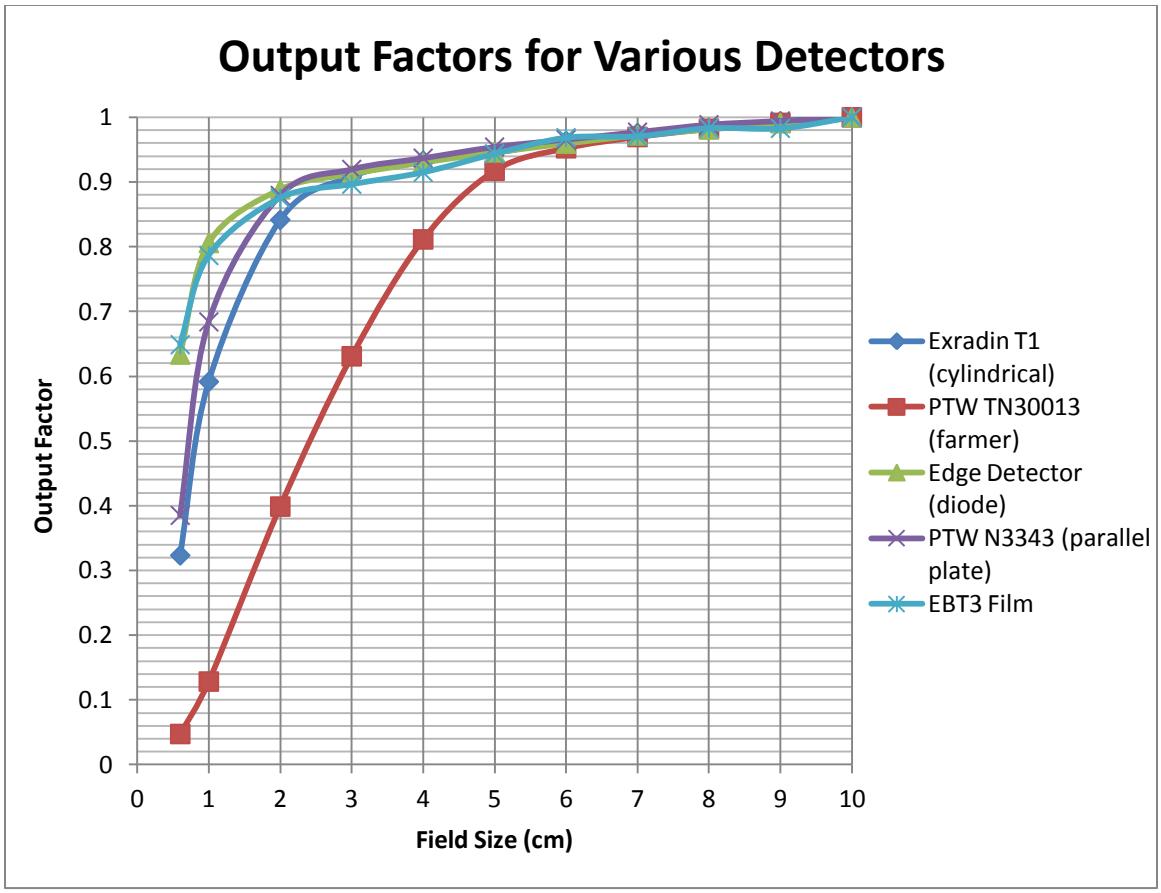

Figure 23 – Output factors measured on Trilogy with 4 different detectors. It can be seen that the edge detector is the only detector used that accurately measured the smaller fields, due to its small enough active volume. No error bars are shown because charge measurements from ion chambers and diodes are extremely consistent.

The only detector here that mimics the expected behavior closely is the Edge Detector (a diode detector), which can serve as a control. It can be seen that all three ion chambers failed to various degrees. The sensitive volumes of the Exradin T1, farmer, and parallel plate chamber used are 0.053cc, 0.6cc, and 0.62cc. These chambers are much too large, and are not accurately measuring small fields due to the volume effect.

It should be noted that the hole that is drilled into the water phantom that was used for the Exradin T1and the PTW TN30013 (Figure 15) ends just at the intersection of the dark lines—meaning that if an ion chamber is placed in the hole and pushed to the end, the tip will just reach this intersection and the sensitive volume is actually just adjacent to it. This was discovered later, and is a partial cause of why the output factors

for those two detectors fell off as far as they did for the smallest fields, where the field is not centered properly on the active area of the detector.

Figure 24 shows a zoomed-in view of the measured output factors for the larger field sizes, showing the increased variation in the film data compared to the ion chambers and diode. Here the linearity in the ion chamber measurements can be more readily seen.

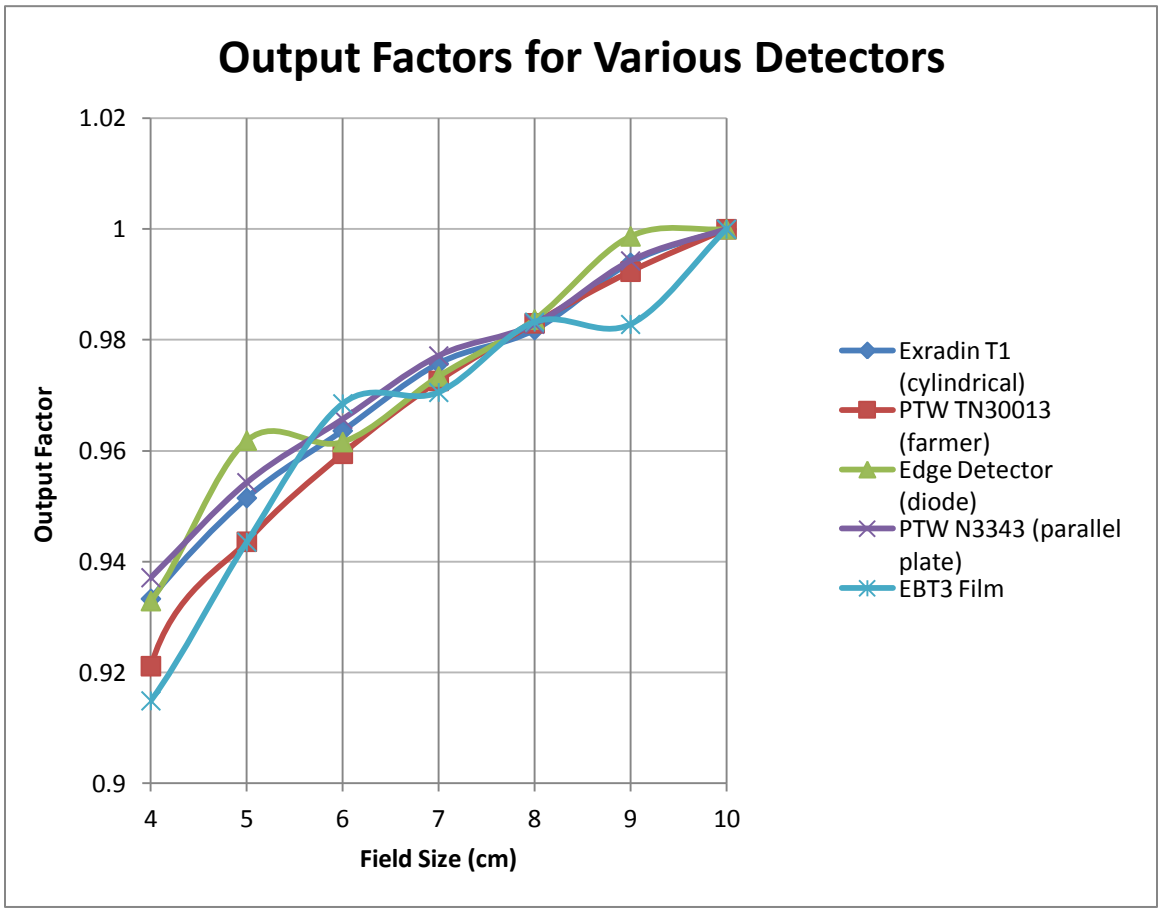

Figure 24 – A zoomed-in view of the measured output factors for the larger field sizes. It can be seen that the both the film and diode data vary slightly more than the ion chamber data.

These measurements with the other non-film detectors were also performed on a Clinac EX and a Trilogy. They are not shown here—for clarity, and redundancy—but are summarized in the following section. All of the raw data are displayed in the additional tables and figures in Appendix B.

4.4 VARIATION BETWEEN LINACS

All of the output factors measured using the different detectors and setups, on the different linacs, are shown as a histogram in Figure 25.

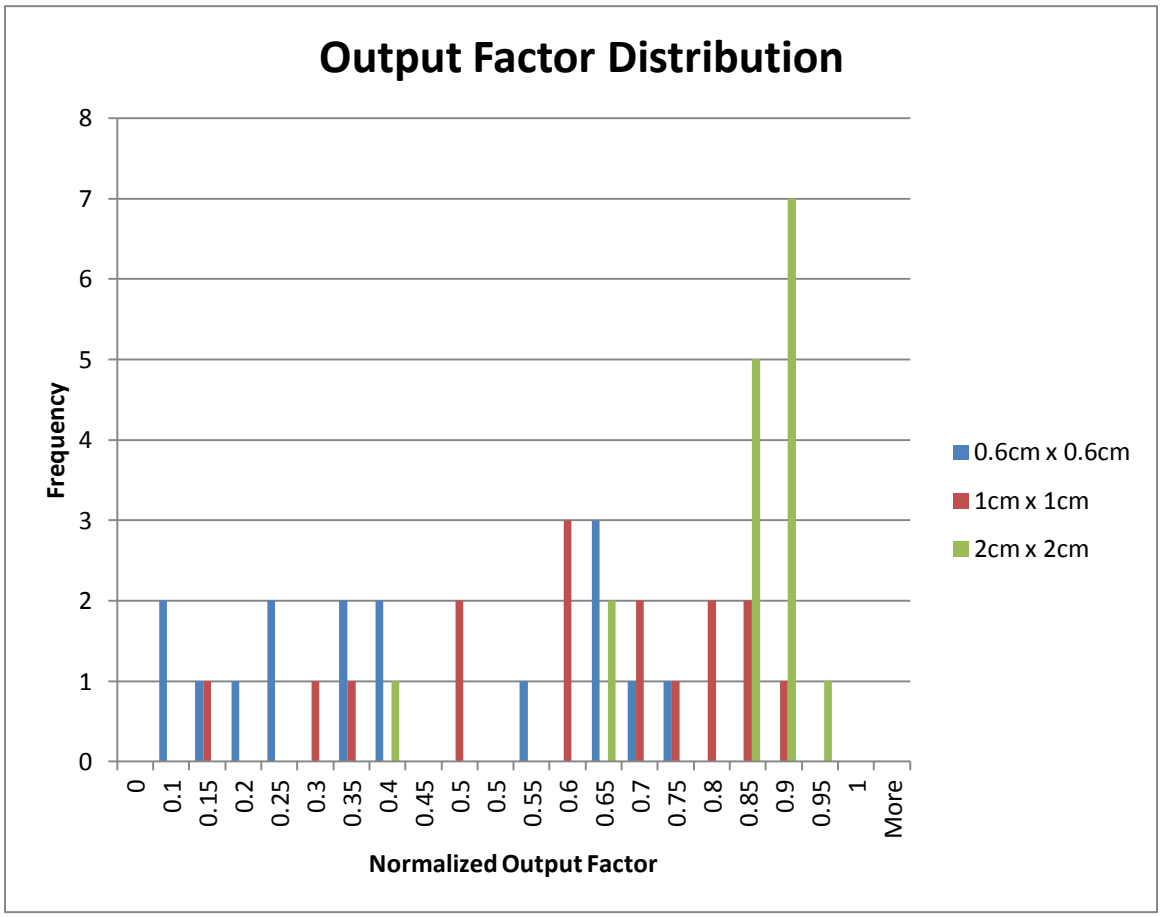

Figure 25 – All the output factors measured, arranged into ranges for comparison.

This histogram can be compared to the data presented by Wolfgang Ullrich, shown in Figure 8. The spread of different output factors obtained for each of the field sizes is much wider here—almost a factor of 4. This is mostly attributable to the variety of detectors used, many of which failed. In order to show a more accurate and realistic variation of output between different linacs, Figure 26 shows another histogram including only the data obtained with the Edge Detector and film:

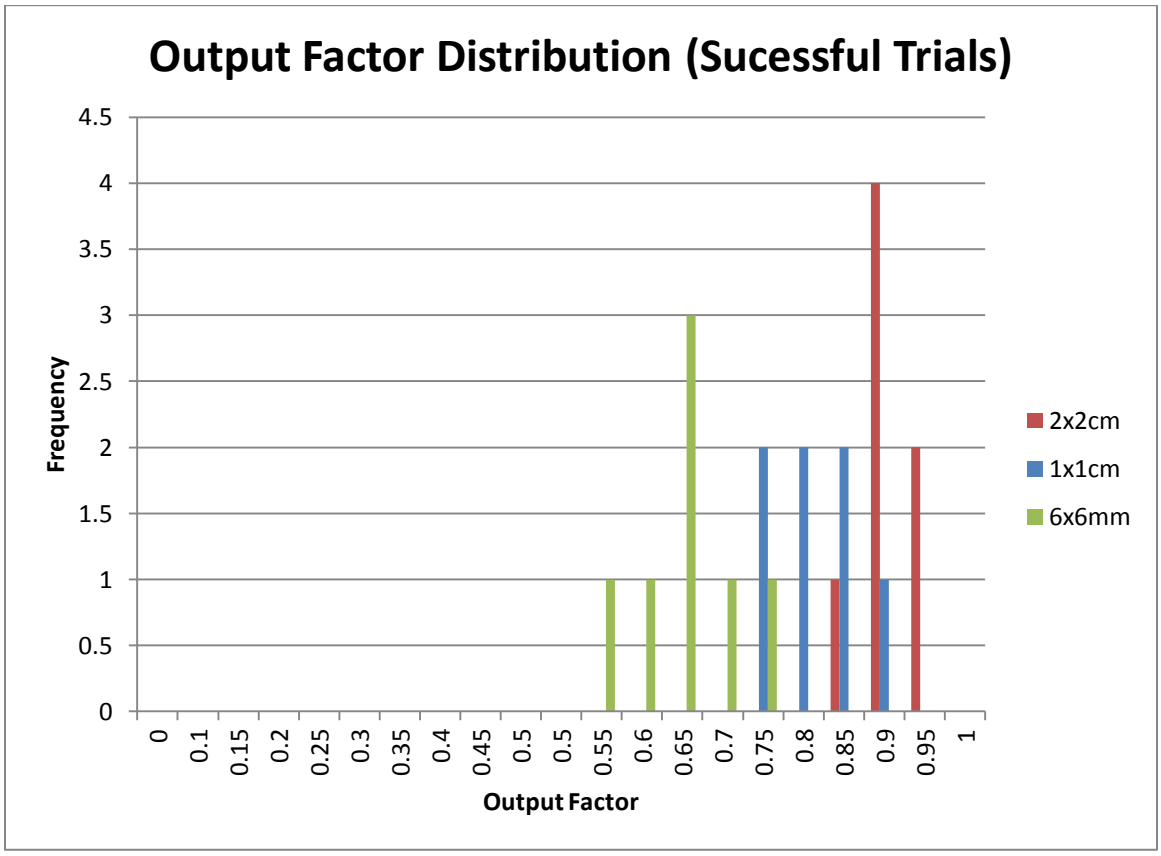

Figure 26 – Output factors from the detectors that are suitable for small fields. A divergence is noted, as well as an increasing divergence for smaller fields.

As shown, the variation is actually *less* than the BrainLab data. It can also be noted that for both Figures 25 and 26 the variation in the output factors increases as the field size gets smaller, as one would expect. It can be seen that the output factors for the 6x6mm field are slightly higher than that of the BrainLAB data, perhaps because only film and the edge detector were considered. Also, the output factors for the 2x2cm field are similar in value (as they should be) to the 18x18mm field size output factor data in the BrainLAB figure.

These data highlight how much the output varies between different linacs. This is why it is necessary to commission treatment planning systems, and why individual clinics need to perform their own small field calibrations—not rely on reference data from other institutes. It is also highlighted why an established Code of Practice to refer to is necessary.

CHAPTER IV
CONCLUSIONS & FUTURE DEVELOPMENTS

When the field size of a beam of radiation gets small enough, the absorbed dose and dose profile change significantly when compared to larger fields. This difference needs to be measured and well understood before these small beams of radiation can be used therapeutically.

Gafchromic EBT3 film was shown to be capable of measuring these small fields due to its superior spatial resolution. The accuracy of other commonly used detectors for the small fields was also investigated. The results show that ion chambers failed badly, while the diode detector performed well. The orientation effect of film is observed, highlighting the need for film to always be scanned in the same orientation. A discrepancy is noted between the dose to the EBT3 film when irradiated at vertical and horizontal orientations. EBT3 film is inexpensive and a good option for smaller clinics that do not have the equipment or personnel to perform more complex small field relative dosimetry.

In the future, treatment machines will likely become more complex and precise—delivering escalated doses of radiation with steeper dose gradients and smaller margins for error. There are a number of AAPM task groups and other international committees working on developing protocols that can be adopted to perform measurements of these small fields, especially in regards to commissioning machines to be used in the clinic. Once these are finalized, there will be established Codes of Practice that can be referred to, which may include reference data such as correction factors for certain commonly used detectors. Until then, it is up to individual clinics to perform these measurements. A simple outline of using film for this purpose is presented here.

New radiation detection tools will likely be developed that are designed for measuring these small fields, which may make it less confusing and dubious to choose a proper detector for certain tasks. Many of these types of tools which exist now—such as diodes and diamond detectors—are already expensive, which may mean future tools will become more expensive. This strengthens the reasons for using film for this purpose.

It is the job of the medical physicist to ensure that every patient receives the best treatment plan possible, and that that plan is delivered in the most accurate way possible. As technology progresses and treatment machines become more complex and powerful, the role of the medical physicist will become more important. In order for the physicist to fulfill this role, a concerted effort must be made to understand newer machines and investigate the software and methods by which they are used—including smaller and more dangerous fields that are inversely planned.

APPENDIX A

DISCREPANCY IN ORIGINAL FILM DATA

Several trials were needed before the output factors measured with the EBT3 film looked correct. These trials were performed on two different linacs, with multiple different calibration films, and the films were scanned multiple times. The following is a brief discussion of what caused the error, for reference. The results from these early three trials are shown in Figure 27.

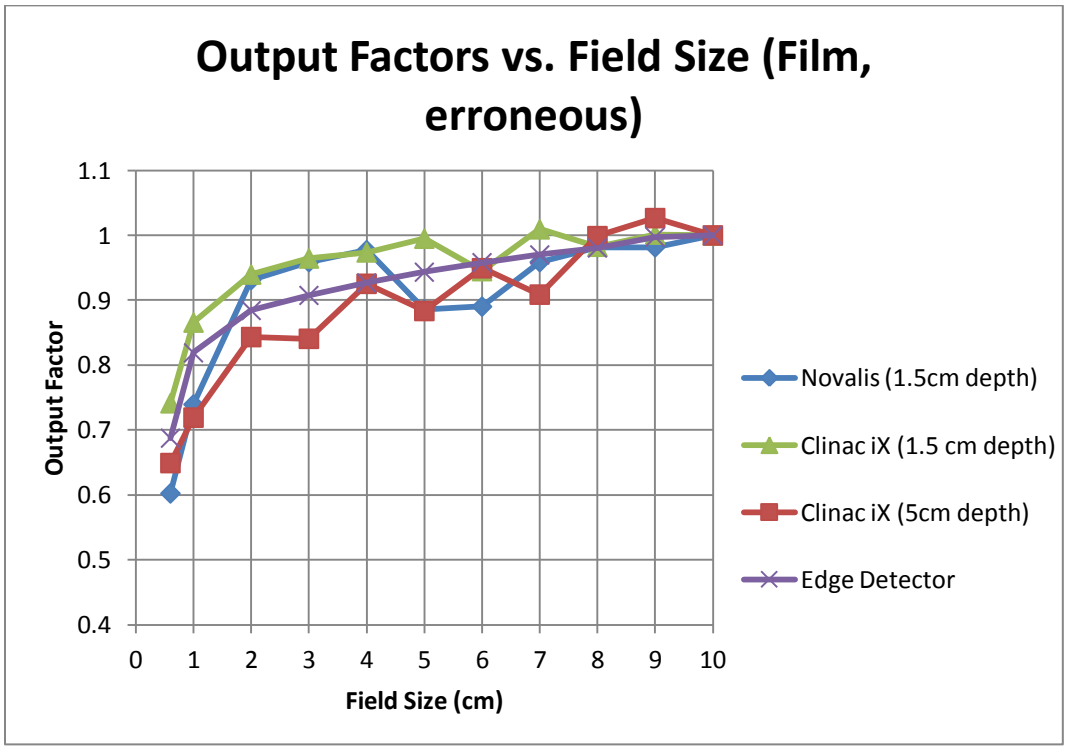

Figure 27 – The original output factors taken from the Georgia Tech Clinac iX and Novalis Tx, using both the 1.5cm and 5cm top solid water blocks. The edge detector data is provided as a control.

The data obtained from a 5cm depth seems to follow an oscillatory pattern. Several of the film output factors are larger than the factors for the 10x10cm^2 field, which shouldn't happen. The diode data, which provides a relatively accurate curve for comparison, depicts a more accurate portrayal of what should happen for the larger fields,

where the dose slowly decreases a small amount with field size. The factors measured with film vary above and below this by as much as 15%. This fluctuation in the dose could be seen from the absorbed dose values originally found. Although we chose not to worry about the dose measurements, the relative comparison between them is important in characterizing the output of the machine.

There is a natural variation in film measurements of anywhere from 2-5%, but this had to have been due to something else because of the variation is significantly larger. Even when taking a mean dose value from a region of interest in the center of the film, as shown earlier, the output factors still fluctuate too much. Because the data are from two different linacs, one of which is actively being used clinically, that rules out the possibility that either machine was not functioning properly. It is known that the darkness of the film increases slightly over time, but again all of the films were scanned together at the same time, so that shouldn't lead to a *relative* variation either.

The systematic search for the causes of the oscillatory pattern eventually pointed to the importance of the orientation of the film when it is scanned (see Section 2.3.5) When the thin film of the active layer of the EBT3 film is deposited, the grains of molecules arrange themselves in a pattern uniformly pointing in a certain direction. This makes the readout direction-dependent when the light is sent through the film during scanning. Therefore, when the original sheet of film is cut up into smaller pieces, it needs to be clear what orientation the smaller pieces are in relation to the original sheet. So when a full sheet is cut down the short way, the two 5x8 cm^2 pieces actually need to be scanned the "short" way in order for them to be scanned in "portrait" orientation, relative to the original sheet of film. To demonstrate this effect in the third trial, on the Novalis, some of the films were cut down into 4x8 cm^2 pieces. These pieces were cut in half again, creating 4x5 cm^2 pieces. Each piece was marked so that the orientation on the couch was clear, and each film was sent the long way ("portrait") downward through the Vidar scanner with that mark in the top right, keeping the orientation the same. Table 3 shows the absorbed dose values from those films, which were also scanned rotated 90 degrees to the right ("landscape").

Table 3. Absorbed dose values from third trial on Novalis

	Portrait	Landscape	
Field size (cm)	Dose (cGy)		Film size (cm)
0.6	132	136	5x8
1	162	168	5x8
2	204	180	4x5
3	210	185	4x5
4	214	188	4x5
5	194	194	4x5
6	195	204	5x8
7	210	210	5x8
8	215	197	8x10
9	215	210	8x10
10	219	200	8x10

For the 8x10 cm^2 and 4x5 cm^2 pieces of film, the dose is reduced when scanned in landscape orientation, by as much as 20%. But for the 5x8 cm^2 pieces, the dose is actually *increased.*

In the fourth and final trial of the film data, the film was not cut up at all. The film was still marked the same way so the orientation relative to the gantry was known, and all films were scanned in true portrait orientation in the same direction. This finally produced more accurate data that agreed with other reports in the literature.

APPENDIX B

RAW OUTPUT FACTOR DATA OBTAINED WITH ION CHAMBERS AND DIODE DETECTOR

Table 4. Raw output factor data obtained on TrueBeam, Trilogy, and Clinac 21EX.

21EX	Detector							
	Exradin T1		PTW TN30013 IC		Edge Detector		PTW N3343 Parallel Plate	
Field Size	Raw (nC)	Normalized	Raw (nC)	Normalized	Raw (nC)	Normalized	Raw (nC)	Normalized
0.6	0.53	0.33125	2.06	0.116912599	26.59	0.687790998	0.66	0.38150289
1	0.94	0.5875	5.41	0.307037457	31.67	0.819192964	1.21	0.699421965
2	1.35	0.84375	11.45	0.649829739	34.19	0.884376617	1.53	0.884393064
3	1.45	0.90625	15.05	0.854143019	35.09	0.907656492	1.58	0.913294798
4	1.49	0.93125	16.2	0.919409762	35.83	0.926797724	1.62	0.936416185
5	1.51	0.94375	16.57	0.940408627	36.47	0.943352302	1.64	0.947976879
6	1.54	0.9625	16.85	0.956299659	37.04	0.958096223	1.67	0.965317919
7	1.56	0.975	17.09	0.969920545	37.5	0.969994827	1.69	0.976878613
8	1.57	0.98125	17.29	0.981271283	37.91	0.980600103	1.7	0.98265896
9	1.59	0.99375	17.47	0.991486947	38.56	0.997413347	1.72	0.994219653
10	1.6	1	17.62	1	38.66	1	1.73	1
TrueBeam	Detector							
	Exradin T1		PTW TN30013 IC		Edge Detector		PTW N3343 Parallel Plate	
Field Size	Raw (nC)	Normalized	Raw (nC)	Normalized	Raw (nC)	Normalized	Raw (nC)	Normalized
0.6	0.33	0.2	1.48	0.081007115	20.34	0.535277244	0.41	0.234285714
1	0.82	0.496969697	4.66	0.255062945	30.29	0.79712624	1.04	0.594285714
2	1.38	0.836363636	11.17	0.611384784	34.05	0.896076213	1.54	0.88
3	1.5	0.909090909	15.14	0.828680898	34.84	0.916866233	1.61	0.92
4	1.54	0.933333333	16.83	0.921182266	35.45	0.932919287	1.64	0.937142857
5	1.57	0.951515152	17.24	0.943623426	36.55	0.961867418	1.67	0.954285714
6	1.59	0.963636364	17.53	0.959496442	36.54	0.961604253	1.69	0.965714286
7	1.61	0.975757576	17.77	0.972632731	36.99	0.97344667	1.71	0.977142857
8	1.62	0.981818182	17.96	0.983032293	37.38	0.983710098	1.72	0.982857143
9	1.64	0.993939394	18.13	0.992337165	37.95	0.998710492	1.74	0.994285714
10	1.65	1	18.27	1	37.999	1	1.75	1
Trilogy	Detector							
	Exradin T1		PTW TN30013 IC		Edge Detector		PTW N3343 Parallel Plate	

Table 4 continued

Field Size	Raw (nC)	Normalized	Raw (nC)	Normalized	Raw (nC)	Normalized	Raw (nC)	Normalized
0.6	0.53	0.323170732	0.87	0.04730832	23.96	0.633527234	0.67	0.385057471
1	0.97	0.591463415	2.36	0.128330614	30.48	0.805922792	1.19	0.683908046
2	1.38	0.841463415	7.33	0.398586188	33.61	0.888683236	1.53	0.879310345
3	1.49	0.908536585	11.6	0.630777597	34.51	0.912480169	1.6	0.91954023
4	1.53	0.932926829	14.92	0.811310495	35.18	0.930195664	1.63	0.936781609
5	1.55	0.945121951	16.87	0.917346384	35.77	0.945795875	1.66	0.954022989
6	1.58	0.963414634	17.51	0.952147906	36.28	0.959280804	1.68	0.965517241
7	1.6	0.975609756	17.83	0.969548668	36.76	0.971972501	1.7	0.977011494
8	1.61	0.981707317	18.06	0.982055465	37.11	0.981226864	1.72	0.988505747
9	1.63	0.993902439	18.23	0.991299619	37.49	0.991274458	1.73	0.994252874
10	1.64	1	18.39	1	37.82	1	1.74	1

Table 5. Raw electrometer data from measurements taken with the Exradin T1.

	Clinac iX		Novalis Tx	
Field Size	Raw (nC)	Normalized	Raw (nC)	Normalized
0.6	0.37	0.232704403	0.55	0.348101
1	0.8	0.503144654	0.94	0.594937
2	1.31	0.823899371	1.34	0.848101
3	1.43	0.899371069	1.43	0.905063
4	1.47	0.924528302	1.47	0.93038
5	1.5	0.943396226	1.50	0.949367
6	1.52	0.955974843	1.52	0.962025
7	1.54	0.968553459	1.54	0.974684
8	1.56	0.981132075	1.56	0.987342
9	1.58	0.993710692	1.57	0.993671
10	1.59	1	1.58	1

REFERENCES

[1] Leksell, L. (1983). Stereotactic radiosurgery. Journal of Neurology, Neurosurgery & Psychiatry, 46(9), 797-803.

[2] Lutz, W., Winston, K. R., & Maleki, N. (1988). A system for stereotactic radiosurgery with a linear accelerator. International Journal of Radiation Oncology* Biology* Physics, 14(2), 373-381.

[3] Blomgren, H., Lax, I., Näslund, I., & Svanström, R. (1995). Stereotactic high dose fraction radiation therapy of extracranial tumors using an accelerator: clinical experience of the first thirty-one patients. Acta Oncologica, 34(6), 861-870.

[4] Levivier M, Gaevart T, Negretti L. Gamma Knife, CyberKnife, TomoTherapy: Gadgets or useful tools? Curr Opin Neurol. 2011;24:616–25.

[5] Das, I. J., Ding, G. X., & Ahnesjö, A. (2008). Small fields: Nonequilibrium radiation dosimetry. Medical physics, 35, 206.

[6] Attix, F. H. (1986). Introduction on radiological physics and radiological dosimetry. Wiley, New York.

[7] Almond, P. R., Biggs, P. J., Coursey, B. M., Hanson, W. F., Huq, M. S., Nath, R., & Rogers, D. W. O. (1999). AAPM's TG-51 protocol for clinical reference dosimetry of high-energy photon and electron beams. Medical physics, 26, 1 847.

[8] PTW Small Field Dosimetry Application Guide

[9] Das, I. Small-Field Dosimetry. Presentation at the 2011 AAPM annual meeting in Vancouver, BC.

[10] Almond, P. R., Attix, F. H., Humphries, L. J., Kubo, H., Nath, R., Goetsch, S., & Rogers, D. W. (1994). The calibration and use of plane-parallel ionization chambers for dosimetry of electron beams: An extension of the 1983 AAPM protocol report of AAPM Radiation Therapy Committee Task Group No. 39. Medical Physics-New York-Institute of Physics, 21(8), 1251-1260.

[11] Wang, L. L., & Leszczynski, K. (2007). Estimation of the focal spot size and shape for a medical linear accelerator by Monte Carlo simulation. Medical physics, 34, 485.

[12] Sham, E., Seuntjens, J., Devic, S., & Podgorsak, E. B. (2008). Influence of focal spot on characteristics of very small diameter radiosurgical beams. Medical physics, 35, 3317.

[13] Jaffray, D. A., Battista, J. J., Fenster, A., & Munro, P. (1993). X-ray sources of medical linear accelerators: Focal and extra-focal radiation. *Medical physics,20*, 1417.

[14] Aspradakis MM, Byrne JP, Palmans H, et al. (2010) IPEM Report Number 103: small field MV photon dosimetry. Institute of Physics and Engineering in Medicine.

[15] Khan, F. M. (2009). The physics of radiation therapy. Lippincott Williams & Wilkins.

[16] Scott, A. J., Nahum, A. E., & Fenwick, J. D. (2009). Monte Carlo modeling of small photon fields: Quantifying the impact of focal spot size on source occlusion and output factors, and exploring miniphantom design for small-field measurements. Medical physics, 36, 3132.

[17] Jones, A. O., & Das, I. J. (2005). Comparison of inhomogeneity correction algorithms in small photon fields. Medical physics, 32, 766.

[18] Ahnesjö, A. (1989). Collapsed cone convolution of radiant energy for photon dose calculation in heterogeneous media. Medical physics, 16, 577.

[19] Du Plessis, F. C. P., Willemse, C. A., Lötter, M. G., & Goedhals, L. (2001). Comparison of the Batho, ETAR and Monte Carlo dose calculation methods in CT based patient models. Medical physics, 28, 582.

[20] Wong, C. J., Ackerly, T., He, C., Patterson, W., Powell, C. E., Qiao, G., ... & Geso, M. (2009). Small field size dose-profile measurements using gel dosimeters, gafchromic films and micro-thermoluminescent dosimeters. Radiation Measurements, 44(3), 249-256.

[21] Andreo, P., Burns, D. T., Hohlfeld, K., Saiful Huq, M., Kanai, T., Laitano, F., ... & Vynckier, S. (2000). IAEA TRS-398. Absorbed Dose Determination in External Beam Radiotherapy: An International Code of Practice for Dosimetry based on Standards of Absorbed Dose to Water.

[22] Sánchez-Doblado, F., Hartmann, G. H., Pena, J., Roselló, J. V., Russiello, G., & Gonzalez-Castano, D. M. (2007). A new method for output factor determination in MLC shaped narrow beams. Physica Medica, 23(2), 58-66.

[23] Laub, W. U., & Wong, T. (2003). The volume effect of detectors in the dosimetry of small fields used in IMRT. Medical physics, 30, 341.

[24] Seuntjens, J. Small Field Dosimetry for IMRT and Radiosurgery (2011). Presented at 2011 SEAAPM annual meeting; April 6-9, Myrtle Beach, SC.

[25] Alfonso, R., Andreo, P., Capote, R., Huq, M. S., Kilby, W., Kjäll, P., ... & Vatnitsky, S. (2008). A new formalism for reference dosimetry of small and nonstandard fields. Medical physics, 35, 5179.

[26] Sauer, O. A., & Wilbert, J. (2007). Measurement of output factors for small photon beams. Medical physics, 34, 1983.

[27] Higgins, P. D., Sibata, C. H., Siskind, L., & Sohn, J. W. (1995). Deconvolution of detector size effect for small field measurement. Medical physics, 22, 1663.

[28] Pappas, E., Maris, T. G., Papadakis, A., Zacharopoulou, F., Damilakis, J., Papanikolaou, N., & Gourtsoyiannis, N. (2006). Experimental determination of the effect of detector size on profile measurements in narrow photon beams. Medical physics, 33, 3700.

[29] Ralston, A., Liu, P., Warrener, K., McKenzie, D., & Suchowerska, N. (2012). Small field diode correction factors derived using an air core fibre optic scintillation dosimeter and EBT2 film. Physics in Medicine and Biology, 57(9), 2587.

[30] Nizin, P. S., & Mooij, R. B. (1997). An approximation of central-axis absorbed dose in narrow photon beams. Medical physics, 24, 1775.

[31] Bednarz, G., Huq, M. S., & Rosenow, U. F. (2002). Deconvolution of detector size effect for output factor measurement for narrow Gamma Knife radiosurgery beams. Physics in medicine and biology, 47(20), 3643.

[32] Kijewski, P. K., Bjärngard, B. E., & Petti, P. L. (1986). Monte Carlo calculations of scatter dose for small field sizes in a Co beam. Medical physics, 13, 74.

[33] Ding, G. X. (2002). Energy spectra, angular spread, fluence profiles and dose distributions of 6 and 18 MV photon beams: results of Monte Carlo simulations for a Varian 2100EX accelerator. Physics in medicine and biology, 47(7), 1025.

[34] Ding, G. X., Duggan, D. M., Coffey, C. W., Shokrani, P., & Cygler, J. E. (2006). First macro Monte Carlo based commercial dose calculation module for electron beam treatment planning—new issues for clinical consideration. Physics in medicine and biology, 51(11), 2781.

[35] Paelinck, L., Reynaert, N., Thierens, H., De Neve, W., & De Wagter, C. (2005). Experimental verification of lung dose with radiochromic film: comparison with Monte Carlo simulations and commercially available treatment planning systems. Physics in medicine and biology, 50(9), 2055.

[36] Al-Hallaq, H. A., Reft, C. S., & Roeske, J. C. (2006). The dosimetric effects of tissue heterogeneities in intensity-modulated radiation therapy (IMRT) of the head and neck. Physics in medicine and biology, 51(5), 1145.

[37] Cheng, C. W., & Das, I. J. (1996). Dosimetry of high energy photon and electron beams with CEA films. Medical physics, 23, 1225.

[38] Chetty, I. J., & Charland, P. M. (2002). Investigation of Kodak extended dose range (EDR) film for megavoltage photon beam dosimetry. Physics in medicine and biology, 47(20), 3629.

[39] Devic, S. (2011). Radiochromic film dosimetry: Past, present, and future. Physica Medica, 27(3), 122-134.

[40] Niroomand-Rad A., Blackwell C. R., Coursey B. M., Gall K. P., Galvin J. M., McLaughlin W. L., Meigooni A. S., Nath R., Rodgers J. E., and Soares C. G. (1998). Radiochromic film dosimetry. Recommendations of AAPM Radiation Therapy Committee Task Group 55. Med. Phys. 25, 2093–2115.

[41] Masi, L., Casamassima, F., Doro, R., & Francescon, P. (2011). Quality assurance of volumetric modulated arc therapy: Evaluation and comparison of different dosimetric systems. Medical physics, 38, 612.

[42] Ju, S. G., Han, Y., Kum, O., Cheong, K. H., Shin, E. H., Shin, J. S., ... & Ahn, Y. C. (2010). Comparison of film dosimetry techniques used for quality assurance of intensity modulated radiation therapy. Medical physics, 37, 2925.

[43] Van Battum, L. J., Hoffmans, D., Piersma, H., & Heukelom, S. (2008). Accurate dosimetry with GafChromic™ EBT film of a 6 MV photon beam in water: What level is achievable?. Medical physics, 35, 704.

[44] Ferreira, B. C., Lopes, M. C., & Capela, M. (2009). Evaluation of an Epson flatbed scanner to read Gafchromic EBT films for radiation dosimetry. Physics in medicine and biology, 54(4), 1073.

[45] Muench, P. J., Meigooni, A. S., Nath, R., & McLaughlin, W. L. (1991). Photon energy dependence of the sensitivity of radiochromic film and comparison with silver halide film and LiF TLDs used for brachytherapy dosimetry. Medical physics, 18(4), 769.

[46] Butson, M. J., Cheung, T., & Yu, P. K. (2006). Weak energy dependence of EBT Gafchromic film dose response in the 50kVp–10MVp X-ray range. Applied radiation and isotopes, 64(1), 60-62.

[47] Rink, A., Vitkin, I. A., & Jaffray, D. A. (2005). Characterization and real-time optical measurements of the ionizing radiation dose response for a new radiochromic medium. Medical physics, 32, 2510.

[48] Sutherland, J. G. H., & Rogers, D. W. O. (2010). Monte Carlo calculated absorbed-dose energy dependence of EBT and EBT2 film. Medical physics, 37(3), 1110.

[49] Saini, A. S., & Zhu, T. C. (2007). Energy dependence of commercially available diode detectors for in-vivo dosimetry. Medical physics, 34, 1704.

[50] Alnawaf, H., Yu, P. K., & Butson, M. (2012). Comparison of Epson scanner quality for radiochromic film evaluation. Journal of Applied Clinical Medical Physics, 13(5).

[51] Lynch, B. D., Kozelka, J., Ranade, M. K., Li, J. G., Simon, W. E., & Dempsey, J. F. (2006). Important considerations for radiochromic film dosimetry with flatbed CCD scanners and EBT GAFCHROMIC film. Medical physics, 33, 4551.

[52] Menegotti, L., Delana, A., & Martignano, A. (2008). Radiochromic film dosimetry with flatbed scanners: A fast and accurate method for dose calibration and uniformity correction with single film exposure. Medical physics, 35, 3078.

[53] Wilcox, E., Daskalov, G., & Nedialkova, L. (2007). Comparison of the Epson Expression 1680 flatbed and the Vidar VXR-16 Dosimetry PRO™ film scanners for use in IMRT dosimetry using Gafchromic and radiographic film. Medical physics, 34, 41.

[54] Syh, J., Patel, B., Wu, H., Rosen, L., Durci, M., Katz, S., & Sibata, C. (2012). SU-ET-135: Investigation of Commercial-Grade Flatbed Scanners and a Medical-Grade Scanner for Radiochromic EBT Film Dosimetry. Medical physics, 39(6), 3734.

[55] Micke, A., Lewis, D. F., & Yu, X. (2011). Multichannel film dosimetry with nonuniformity correction. Med Phys, 38(5), 2523-2534.

[56] Hayashi, N., Watanabe, Y., Malmin, R., & Kato, H. (2012). Evaluation of triple channel correction acquisition method for radiochromic film dosimetry. Journal of Radiation Research.

[57] Crijns, W., Maes, F., van der Heide, U. A., & Van den Heuvel, F. (2013). Calibrating page sized Gafchromic EBT3 films. Medical physics, 40, 012102.

[58] Lewis, D., Micke, A., Yu, X., & Chan, M. F. (2012). An efficient protocol for radiochromic film dosimetry combining calibration and measurement in a single scan. Medical physics, 39, 6339.

[59] E. E. Klein, J. Hanley, J. Bayouth, F. F. Yin, W. Simon, S. Dresser, C. Serago, F. Aguirre, L. Ma, B. Arjomandy, C. Liu, C. Sandin, and T. Holmes. (2009) Task Group 142 report: Quality assurance of medical accelerators. Med. Phys. 36, 4197–4212.